The Delayed Response of Airborne Thermometers: Effect on Measuring the Flux of Sensible Heat

William A. Cooper and others...

DRAFT May 2020

National Center for Atmospheric Research
Earth Observing Laboratory
Research Aviation Facility

Table of Contents

1 Introduction **1**

2 Determining the Transfer Function **2**

2.1 Theory 2

2.2 The response to dynamic heating 6

2.3 Data sources 6

2.4 Fits to the measurements 7

2.5 Response to a step change 14

2.6 Uses of the transfer functions 14

3 Correcting for Dynamic Heating **16**

3.1 A filter for dynamic heating 17

3.2 Other filtering methods 19

4 The Flux of Sensible Heat **23**

4.1 Outline of the correction procedure 23

4.2 Examples of Measured Cospectra and Fluxes 24

4.3 Evidence from Simulated Measurements 26

5 Summary and Conclusions **30**

A Correcting the Temperature **32**

B The Digital Filter for Dynamic Heating **38**

C Pressure-Line Resonance **39**

D Reproducibility **44**

References **45**

List of Figures

1 The amplitude and phase for the frequency domain transfer function of the Rosemount 102E4AL temperature sensor 5

2 (top): Phase of measured recovery temperature relative to dynamic heating, for the measurements (with error bars) and for the theoretical response for the best-fit parameters (green line). The error bars indicate two-standard-deviation ranges in the mean at each plotted point. Data from the flight segments listed in Table 1.
(bottom): The ratio of the spectral amplitude for the measurement of recovery temperature ($T_m(t)$) to that for dynamic heating (Q), shown as the plotted data points. There are additional data points at frequencies below about 0.04 Hz that do not appear in this plot because they lie above the upper limit for the ordinate. The green line is the prediction from the transfer function determined from the best-fit values matching the phase lag between these variables, and the dashed orange line is a similar result with the second time constant τ_2 increased from 0.447 to 0.6 s to illustrate sensitivity to this parameter. 9

3 Spectral variance $P(\nu)$ weighted by frequency (ν) for the recovery temperature measured by a heated HARCO and an unheated Rosemount sensor 11

4 The phase (top) and gain (bottom) for the transfer function characterizing a heated HARCO temperature sensor. The measurements are indicated by error bars that show two-standard-deviation limits from the mean value). Two fits to the measurements, one based on the three-parameter representation ("3-par") and one on a polynomial fit ("lfit"), are described in the text. 12

5 (blue dots) 15

6 The weighted variance spectrum as a function of frequency ν for the recovery temperature measured by a Rosemount 102E4AL sensor 16

7 (a) The impulse response function found from the inverse Fourier transform of the transfer function for the unheated Rosemount 102E4AL sensor (Rosemount) and for the heated HARCO sensor (HARCO), using the response parameters from Table 2 of Part 1 18

8 Variance spectra for the unheated Rosemount 102E4AL sensor, for the same flight segment used for Fig. 6.
Left, (a): The dynamic-heating term ("Q:) and for the filtered term obtained by integrating the differential equations for the derivatives ("DiffEq"), by Fourier transformation with application of the transfer function ("FFT"), or applying the digital filter ("filter"). The result for the latter is so close to that for "FFT" that it is obscured in this plot.
Right, (b): The measurement of recovery temperature and ambient temperature calculated using the filtered dynamic-heating term. The original variable for ambient temperature based on standard processing is also shown. 20

9 Variance spectra for the heated HARCO sensor.
Left, (a): The unmodified dynamic-heating term ("Q") and the two filtered terms. The results from solving the differential equations ("DiffEq") or from application of the digital filter ("filter") are overlapping and indistiguishable in this figure.
Right, (b): The temperature as modified by filtering the dynamic-heating term (blue line). The other plotted spectra are for the measured recovery temperature and the air temperature with the conventional dynamic-heating correction. . . . 21

10 Comparison of the original measured temperature and the same temperature after filtering the dynamic-heating correction:
(left): An unheated Rosemount 102E4AL sensor; (right): A heated HARCO sensor. . . . 22

11 (top): The corrected flux of sensible heat for SOCRATES flight 15, 6:00:00 to 6:15:00, a low-level flight segment over the southern-hemisphere ocean. The "exceedance" is the complement of the cumulative distribution function (i.e., the sum of contributions from frequencies above the plotted value), and the dashed brown exceedance line is that without transfer-function correction but with adjustment of the dynamic-heating term to incorporate the estimated response of the temperature sensor.
(bottom): Cospectrum for the flux of sensible heat, for three 10-min flight segments from the CSET project. The dashed brown line is the exceedance distribution before correction, which gives a flux of 3.07 W m${-2}$ for wavelengths smaller than 2 km and 2.06 W m^{-2} for frequencies above 0.01 Hz. . . . 25

12 The cospectrum for the flux of sensible heat (blue line), weighted by frequency ν, for the simulated data generated as described in the text . . . 28

13 Example of the changes produced by the correction procedures . . . 33

14 Variance spectra for the original measurement of recovery temperature (Tm) produced by an unheated Rosemount sensor and for the corrected values (RT and FFT) produced respectively by (16) and the Fourier-transform algorithm . . 34

15 Corrected recovery temperature as measured by a heated HARCO sensor ("RTH" and "FFT"), the uncorrected measurement ("Tm"), and the best estimate of the true recovery temperature ("RT") based on an unheated Rosemount sensor after correction . . . 36

16 Variance spectra for some measurements of recovery temperature . . . 37

17 The variance spectrum for the dynamic-heating correction Q, from SOCRATES flight 15, 6:00:00 to 6:15:00 UTC, in a region thought to have characteristics of an inertial subrange . . . 40

18 Variance spectra for three pressure measurements . . . 41

19 The variance spectrum that results from correcting the measured static pressure ("PS") for the theoretical effect of line resonance . . . 42

20 Variance spectra for the best estimate for dynamic heating, "QC", after correction for resonance in both lines connected to the differential pressure sensor that produces the original measurement "Q" 43

List of Tables

1 Flight segments from flight 3 of the VOCALS project, 21 October 2008. Listed times are UTC. 8

2 Flight segments used to determine the response characteristics of a heated HARCO sensor. 11

3 Parameters for the time response of available temperature sensors on the NSF/NCAR aircraft, adjusted to $Z = 0.3$. For other conditions, scale as represented for τ_1' in (13). 14

Preface and Abstract

Most measurements of temperature from research aircraft rely on sensors that have inadequate response for the most demanding applications, including especially measurements of the flux of sensible heat. This paper discusses three aspects related to the time response of airborne sensors. First, it uses a new method to characterize the time response in terms of the frequency-domain transfer function; then it demonstrates that standard data processing introduces errors in measured air temperature by exaggerating the influence of dynamic heating on temperature sensors; and finally it uses these results to propose a correction scheme to improve measurements of the flux of sensible heat. Initially, the transfer function describing the time response of two standard airborne thermometers is found by observing the response to turbulent dynamic heating in regions where that is the dominant cause of fluctuations in the measurement. Differential equations for the response are consistent with the observed transfer function, and the observations constrain the parameters in those differential equations with low uncertainty. The transfer functions can then be inverted to obtain corrected measurements of the recovery temperature. They also predict how sensors will respond to fluctuations in the recovery temperature, and those predictions demonstrate that the sensed recovery temperature often does not respond to high-frequency components imposed by dynamic heating. Therefore, the common practice of subtracting the full dynamic heating to obtain the air temperature from the recovery temperature introduces errors that can be especially significant for heated sensors that are inherently slow. The correction procedure developed in the last section is based on using the transfer function to correct the measured recovery temperature before correcting for dynamic heating. The over-arching goal is to be able to assess errors that might be present in measurements of the flux of sensible heat and to apply corrections for those errors. Examples and a simulation illustrate that, without correction, measurements of sensible-heat flux with an unheated Rosemount 102E4AL sensor can be more than 30% too low, but the proposed correction procedure removes this error and results in reliable measurements with negligible error attributable to the response time of the sensor.

Acknowledgements

This material is based upon work supported by the National Center for Atmospheric Research, which is a major facility sponsored by the National Science Foundation under Cooperative Agreement No. 1852977. Any opinions, findings and conclusions or recom-mendations expressed in this publication are those of the author(s) and do not necessarily reflect the views of the National Science Foundation. Measurements used here (UCAR/NCAR - Earth Observing Laboratory [2011], UCAR/NCAR - Earth Observing Laboratory [2019], UCAR/NCAR - Earth Observing Laboratory [2018]) were collected in research projects (Wood et al. [2011], Albrecht et al. [2019], McFarquhar et al. [2014]) that used the NSF/NCAR research aircraft. Project descriptions and additional information can be found at this URL. The referenced project teams conducted the experiments, with flight operations, data acquisition and processing, and other project support by the Research Aviation Facility, Earth Observing Laboratory, National Center for Atmospheric Research (NCAR). The analyses reported here were mostly performed using R (R Core Team [2019]), with RStudio (RStudio [2009]) and knitr (Xie [2013, 2014]). Data files in netCDF format have been read and written using the R package "ncdf4"; cf. Pierce [2015]. Substantial use also was made of the "ggplot2" package (Wickham [2009]) for R, and extensive use was made of the "stats" package, part of Core R. Some of the numerical integrations used the Runge-Kutta function from the "rmutil" package (Swihart and Lindsey [2019]).

1 Introduction

Research aircraft routinely measure air temperature, but the standard sensors do not respond fast enough to meet many scientific needs. In particular, measurements of the flux of sensible heat need faster response than is typically available, as do measurements of near-discontinuous changes such as those at the top of boundary layers or at cloud boundaries. The measurement of sensible-heat flux requires, for the standard eddy-correlation measurement, that temperature be measured with sufficient response to resolve the spectrum of contributions to the flux. Various recent reviews of priorities for research in atmospheric science have called attention to the important roles that fluxes of various quantities play in climate science and have advocated increased focus on those fluxes; e.g., National Research Council [1998].

The basis for the measurement of the flux of sensible heat (F_s) by eddy correlation is this equation:

$$F_s = \rho_a C_p \left\langle w'T' \right\rangle \tag{1}$$

where ρ_a is the density of air, C_p the specific heat of air at constant pressure, w the vertical wind, and T the temperature. Primes in this equation denote fluctuations from the mean and angle brackets denote an ensemble average. The measurement thus depends on having a temperature sensor that can respond to the range of fluctuations making significant contributions to the heat flux. Friehe and Khelif [1992] suggested that 4–5 Hz is "just adequate" (for flight at around 125 m/s) and that 25 Hz would be desirable to resolve some interesting aspects of the temperature structure. If the response of the temperature sensor is reduced or shifted in phase at a particular frequency, an error will be introduced into the measurement of sensible-heat flux. Lawson and Rodi [1992] argued that sensible-heat flux measured by some of the fastest sensors then in common use produced measurements of sensible heat flux about 21% too low compared to the measurements from their faster thermocouple-based sensor. To avoid significant errors in this measurement, it therefore is essential to characterize the time response of the temperature sensor used and, where necessary, to apply corrections to compensate for that response.

2 Determining the Transfer Function

In this first section, the time response of some standard airborne temperature sensors is characterized in terms of a frequency-domain transfer function that relates the measurand (the recovery temperature) to the measurement (the sensor output) in ways that are invertible. Two coupled differential equations with three parameters are proposed as the basis for this characterization, but the transfer function is determined independent of those equations. Because the equations predict a transfer function matching the observations, they provide a useful generalization when the measurements are fitted to a three-parameter equation consistent with those equations. The measured transfer functions then are used in the sections that follow to access how common measurements are affected.

2.1 Theory

The errors considered here apply to the measurement from the sensor, the "recovery temperature," rather than the final temperature after correction for dynamic heating. Because the sensor cannot respond to rapid fluctuations, the standard correction for dynamic heating introduces errors into the measured air temperature that are then amplified by a correction procedure. This will be addressed in the next section, but for this reason the present section will discuss only the recovery temperature.

Payne et al. [1994] provided a particularly illuminating analysis of the expected response of a temperature sensor and developed their results in terms of a transfer function. They represent the response of the sensor in terms of two coupled differential equations, one representing the temperature of the sensing wire and a second representing the temperature of the structure that supports that wire. Their analysis in terms of fundamental representation of the heat transport leads to reasonable consistency with previous two-time-constant models like that of McCarthy [1973] but poor agreement with the empirical evidence regarding the time-response parameters in those models. They note, however, that the empirical evidence is not as consistent or convincing as would be desirable. One goal of the present work is to develop a different and readily available method of determining those parameters.

Previous studies have demonstrated that a simple first-order exponential equation with one time constant does not represent the time response of airborne temperature sensors. The suggested explanation (Lenschow [1972] is that heat is transferred to the sensing wire of standard sensors not only from the air but also from the supporting structure that is in contact with the wire. Friehe and Khelif (Friehe and Khelif [1992]), following other prior work including that of Rodi and Spyers-Duran [1972] and McCarthy [1973], suggested representing the two-time-constant response via the following functional form:

$$\Theta(t) = A_1 e^{-t/\tau_1} + A_2 e^{-t/\tau_2} \tag{2}$$

where $\Theta(t)$ is the normalized history of the measured temperature decaying from an initial value of unity to a final value of zero. The sum of the coefficients A_1 and A_2 must then be 1. The values for $\{A_1, A_2, \tau_1, \tau_2\}$ suggested by Friehe and Khelif [1992] were {0.65, 0.35, 0.09 s, 0.5 s}.

Following the approach of Payne et al. [1994], the time response of the sensor will be represented by two coupled differential equations, one that describes the response of the support on which the sensing wire is wound to the air temperature and a second that describes the response of the sensing wire to two inputs, one from the support and one from the air. No attempt is made here to determine the parameters from first principles as in Payne et al. [1994], however; instead, parameters entering the equations are determined empirically. The equations are:

$$\frac{dT_s(t)}{dt} = \frac{T_r(t) - T_s(t)}{\tau_2} \tag{3}$$

$$\begin{aligned} \frac{dT_m(t)}{dt} &= \frac{a(T_r(t) - T_m(t)) + (1-a)(T_s(t) - T_m(t))}{\tau_1} \\ &= \frac{\{aT_r(t) + (1-a)T_s(t)\} - T_m(t)}{\tau_1} \end{aligned} \tag{4}$$

where $T_s(t)$ is the temperature of the support, $T_m(t)$ the measured temperature of the sensing wire, and $T_r(t)$ the true recovery temperature that is the measurand. For heat transfer to or from the wire, the parameter a then represents the fraction of the heat transferred by the air, while $(1-a)$ is transferred to or from the support. The wire responds to the combined transfers of heat with characteristic time constant τ_1 while the support structure responds to the air temperature more slowly, with time constant τ_2. It is straightforward to apply (3) and (4) to changing but not necessarily discrete conditions, so a general response to a given air-temperature history can be predicted by numerical integration of these equations. Furthermore, the equations are linear and, for constant values of the parameters, they are also time-invariant (i.e., "LTI") descriptions of the response. As a result, a particular signal for $T_r(t)$ can be decomposed into its sinusoidal Fourier components and each will satisfy these equations independently. The first equation does not involve the measurement, so for a particular history of recovery temperature $T_r(t)$ the support temperature can be determined solely by integration of (3). Then, with $T_s(t)$ determined, (4) can be integrated to find the expected measurement $T_m(t)$ for a specified measurand history $T_r(t)$. The inverse process, finding $T_r(t)$ from the measurements $T_m(t)$, is also straightforward and only slightly more complicated, as discussed in Appendix A.

For a sinusoidal input these equations have analytic solutions after any transient response from initial conditions has decayed. If the actual recovery temperature is $T_r(t) = \sin \omega t$ where ω is the angular frequency, then the solutions for $T_s(t)$ and $T_m(t)$ are given by the following equations:

$$T_s(t) = b \sin(\omega t + \zeta) \tag{5}$$

$$T_m(t) = c \sin(\omega t + \phi) = C_1 \cos \omega t + C_2 \sin \omega t \tag{6}$$

where

$$b = \frac{1}{\sqrt{1 + \omega^2 \tau_2^2}}$$

$$\zeta = -\arctan(\omega \tau_2)$$

$$C_1 = \frac{-\omega}{(1+\omega^2\tau_1^2)}\left(\tau_1 a + \frac{(1-a)(\tau_1+\tau_2)}{(1+\omega^2\tau_2^2)}\right)$$

$$C_2 = \left(\frac{1}{1+\omega^2\tau_1^2}\right)\left(a + \frac{(1-a)(1-\omega^2\tau_1\tau_2)}{(1+\omega^2\tau_2^2)}\right)$$

$$c = \sqrt{C_1^2 + C_2^2} \tag{7}$$

$$\phi = \arctan(C_1/C_2) \tag{8}$$

McCarthy [1973] used the derivative of the step-function response to find the impulse response function and, from its Fourier transform, the sensor response function. That leads to the following alternate expressions for C_1 and C_2:

$$C_1 = -\omega\left(\frac{A_1\tau_1}{1+\omega^2\tau_1^2} + \frac{A_2\tau_2}{1+\omega^2\tau_2^2}\right)$$

$$C_2 = \left(\frac{A_1}{1+\omega^2\tau_1^2} + \frac{A_2}{1+\omega^2\tau_2^2}\right)$$

With $A_2 = (1-a)/(1-\tau_1/\tau_2)$ and $A_1 = 1-A_2$, these are equivalent to the expressions for the same coefficients given above (7). This demonstrates that the equations (3) and (4) are a representation of the response equivalent to (2) and to the equations used by McCarthy [1973] and Inverarity [2000], among others.

The transfer function $H(\omega) = c(\omega)e^{i\phi(\omega)}$ then characterizes how the sensor will respond to a unit-amplitude sine wave with angular frequency $\omega = 2\pi\nu$ where ν is the frequency. For a particular set of parameters (a =0.733, τ_1 =0.0308 s, τ_2 =0.447 s),[1] the amplitude response and phase delay of the transfer function are shown in Fig. 1. Similar plots of the amplitude (but not the phase) have been shown by McCarthy [1973] and Nicholls [1978]. Modified transfer functions for two small changes to these parameters are also shown to illustrate the sensitivity of the solution to these parameters. This figure illustrates that serious errors will enter estimates of the sensible heat flux if temperature fluctuations at frequencies above 1 Hz make a significant contribution to the flux. The contribution to the cospectrum of temperature and vertical wind will be reduced by the product of the amplitude and the cosine of the phase so at 10-Hz the error is about 86%, but even at 1 Hz the error is about 28%.

These equations and their solution provide a basis for correcting either the measured temperature or the sensible-heat flux calculated from the cospectrum in (1). Corrected values can be obtained by several methods including integration of the equations for the derivatives or by dividing the Fourier transform of the time series by the transfer function and then using inverse Fourier transformation to recover the corrected time series. Those correction schemes are discussed in detail in Appendix A. To support such corrections, the next section determines the transfer function experimentally.

[1] These parameters are approximately representative of an unheated Rosemount 102E4AL sensor used on the NSF/NCAR C-130, as will be demonstrated in Sect. (2.4.1).

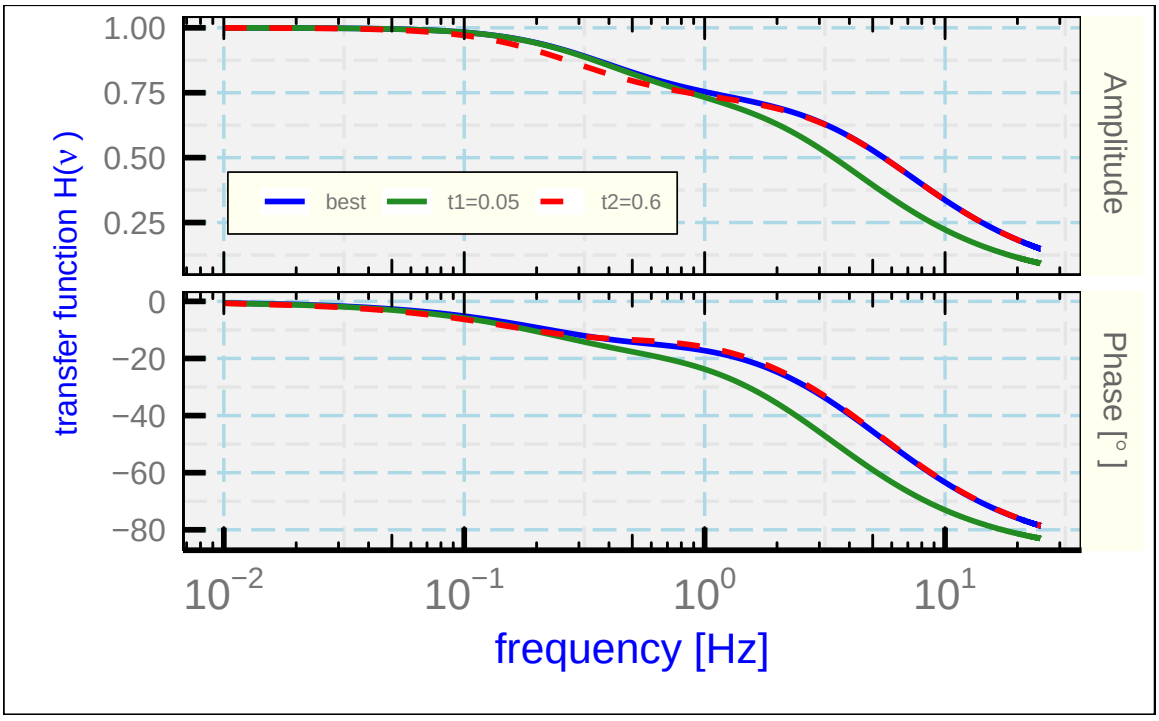

Figure 1: The amplitude and phase for the frequency domain transfer function of the Rosemount 102E4AL temperature sensor. The parameters representing that sensor, labeled "best", are a=0.733, $\tau_1 = 0.0308$ s and $\tau_2 = 0.447$ s. To illustrate sensitivity, the curves labeled "t1=0.05" and "t2=0.6" use instead $\tau_1 = 0.05$ s and $\tau_2 = 0.6$ s, respectively.

2.2 The response to dynamic heating

The evaluation of the time response that follows relies on the dynamic heating produced by airspeed fluctuations. In steady conditions a temperature sensor exposed to the air stream will measure the recovery temperature, defined as the ambient temperature increased by the effect of dynamic heating. Dynamic heating fluctuates as the airspeed fluctuates, so in a turbulent wind field fluctuations with a measurable frequency spectrum are imposed on the sensor. These fluctuations are often significantly larger than real fluctuations in the ambient temperature. Dynamic heating of temperature sensors is discussed for example by Bange et al. [2013] (cf. their Eq. 2.23), who express dynamic heating Q as

$$Q = \alpha_r \frac{V^2}{2C_p} = T_r \left(\frac{\alpha_r M^2 R_a/(2C_v)}{1 + \alpha_r M^2 R_a/(2C_v)} \right) \tag{9}$$

where α_r is the "recovery factor" characterizing the extent to which the air is brought to rest relative to the sensor, V is the airspeed, C_p and C_v are respectively the specific heat of air at constant pressure and constant volume. T_r is the (true) recovery temperature expressed in absolute units, M the Mach number, and R_a the gas constant for air. The ambient air temperature T_a is related to the recovery temperature and the dynamic heating via

$$T_r = T_a + Q \ . \tag{10}$$

Because dynamic heating can exceed 20°C at jet-aircraft flight speeds, it is often the dominant cause of fluctuations in the recovery temperature. If the fluctuations in dynamic heating are higher in frequency than those to which the sensor can respond, corresponding fluctuations will be attenuated in the measured spectrum and the phase of the measured response relative to the imposed signal will vary, from near 0° for fluctuations slow compared to sensor response to near 90° or even more[2] for fluctuations fast compared to that response. The amplitude and phase of the recovery temperature relative to the dynamic-heating forcing therefore can be used as sensitive indicators of the response characteristics of the sensor and can constrain parameters like a, τ_1 and τ_2 that fit the predictions to the observations. The evaluation in terms of the amplitude ratio and phase shift of the recovery temperature in response to dynamic heating will be used to characterize the transfer function and to determine if it is represented adequately by the parameterized form given by (7) and (8).

2.3 Data sources

The present investigation uses measurements from two NSF/NCAR (National Science Foundation / National Center for Atmospheric Research) research aircraft, a Gulfstream V (hereafter, GV) and a Hercules C-130. The temperature sensors producing the measurements are in widespread use so these results should have broad applicability. Some aspects of the uncertainty limits associated with these measurements of temperature are included in an NCAR Technical Note (Cooper et al. [2016]), which focused on the measurements of wind from the

[2] A sensor with a first-order time constant cannot produce a phase lag of more than 90°, but larger lags are possible for systems characterized by two time constants.

GV. That document included an estimate that the standard uncertainty in measurements of temperature from the GV is about 0.3°C and referenced Cooper et al. [2014] for supporting evidence. This limit applies when the temperature being measured is varying slowly but does not apply when the temperature changes rapidly. It is well known, however, that temperature sensors in common use on research aircraft have time-response characteristics that can affect the measurements. Friehe and Khelif [1992] and Lawson and Rodi [1992], among many others, provide reviews of the evidence for delayed response of the standard sensors. In particular, the unheated Rosemount 102E4AL sensor has been used widely as a fast-responding sensor, so it will be a focus of this three-part study.

This research uses data archives produced by three research projects, the VOCALS (VAMOS Ocean-Cloud-Atmosphere-Land Study), CSET (Cloud Systems Evolution in the Trades) and SOCRATES (Southern Ocean Clouds, Radiation, Aerosol Transport Experimental Study) experiments. The field projects are described by Wood et al. [2011], Albrecht et al. [2019] and McFarquhar et al. [2014], respectively. All included low-level flight segments over the Pacific Ocean that are used in this paper. The reference list includes appropriate DOI references to the measurements.

2.4 Fits to the measurements

Because the airspeed V is itself conventionally determined using the processed air temperature T_a, via $V = M\sqrt{\gamma R_a T_a}$ where $\gamma = C_p/C_v$, the second expression in (9) provides the advantage that it does not rely on prior calculation of the air temperature T_a but can be calculated from only the recovery temperature T_r and the Mach number. The Mach number in turn depends only on measurements of the dynamic and ambient pressures, with a small adjustment for the water vapor pressure. However, the available measurement is not the true recovery temperature T_r but instead the measured temperature T_m which may not include high-frequency fluctuations in T_r. This in turn affects the estimated fluctuations determined from (9). To minimize this problem, regions were sought where the fluctuations in dynamic heating were the dominant cause of fluctuations in recovery temperature. Temporarily consider these approximations: $\alpha_r \approx 1$, $R_a/(2C_v) \approx 1/5$, and M small enough that the denominator of the right side of (9) can be assumed equal to unity. Dynamic heating then is approximately $Q \approx T_r M^2/5$ and fluctuations in Q are related to those in T_r and M according to

$$\frac{\delta Q}{Q} \approx \frac{\delta T_r}{T_r} + \frac{2}{5}\frac{\delta M}{M} \tag{11}$$

Because the measured recovery temperature T_m may not include true high-frequency fluctuations in T_r, the measured phase and amplitude of the response to the dynamic-heating term may be distorted from the correct value at frequencies where $\delta T_m/T_m$ differs from $\delta T_r/T_r$. In regions where the last term in (11) dominates, underestimation of the fluctuations in the recovery temperature arising from sensor response will cause less significant errors in the measured fluctuations in dynamic heating Q, and those errors can be addressed by correction procedures.

For a representative low-level flight segment with moderate turbulence where the airspeed fluctuations were approximately consistent with an eddy dissipation rate of $3 \times 10^{-4}\,\mathrm{m^2 s^{-3}}$, the

variance of the second term in (11) is more than 100 times that of the first, indicating that the fluctuations in the first term are less than 10% of those in the second term. Therefore the right side of (9) with T_m in place of T_r was used initially to represent dynamic heating. Once a set of parameters was determined, $T_r(t)$ was calculated using the first correction procedure discussed in Appendix A. Using this estimate of $T_r(t)$ in place of $T_m(t)$ led to a small change in the fitted values of the parameters, but the estimate became stable after only one iteration.

2.4.1 The unheated Rosemount 102E4AL sensor

Segment	start	end
1	6:50:00	7:00:00
2	7:33:00	7:43:00
3	10:46:00	10:56:00
4	11:42:00	11:52:00
5	12:43:00	12:53:00
6	13:30:00	13:40:00

Table 1: Flight segments from flight 3 of the VOCALS project, 21 October 2008. Listed times are UTC.

To characterize the response of the Rosemount 102E4AL sensor, six ten-minute low level flight segments in the marine boundary layer from one flight of the NCAR/NSF C-130 in the "VOCALS" project (Wood et al. [2011]), which studied low-level clouds over the Pacific Ocean near Chile, were selected that had simular flight conditions including the intensity of the turbulence. The time intervals are listed in Table 1. For each flight segment, the phase and amplitude ratio between the measurement and the dynamic heating term were calculated,[3] and the results for all six segments were averaged in 200 logarithmically spaced intervals in frequency. The results for the average phase are shown in Fig. 2a. The theoretical curve is based on best-fit parameters as determined from these measurements and those of the amplitude ratio, discussed next.

The ratio of the amplitude of the response to that of the dynamic-heating signal, used as an estimate of the gain of the transfer function, is shown in Fig. 2b. It is useful to consider both the amplitude and phase when determining the response parameters because, as shown in Fig. 1, the amplitude of the transfer function is more sensitive to τ_2 than the phase but τ_1 is a very sensitive predictor of the phase at high frequency. For the set of favored parameters, Fig. 2b shows the standard prediction and another with τ_2 set to 0.6 s instead, to show the sensitivity of this result to that parameter. The best prediction based on the measured phases consistently underestimates the ratio of spectra for frequencies below about 0.1 Hz and above about 3 Hz but is reasonably consistent with the observed ratio between 0.1 Hz and 3 Hz. Below 0.1 Hz it appears likely that the sensor is responding to real fluctuations in temperature not attributable to dynamic heating, as would be expected at these low frequencies. Above 3 Hz the prediction is much too low, probably because there is noise or other spurious variance in $T_m(t)$ not caused by dynamic heating.

[3]The R routine "spec.pgram()" was used with 25-point modified Daniell smoothing.

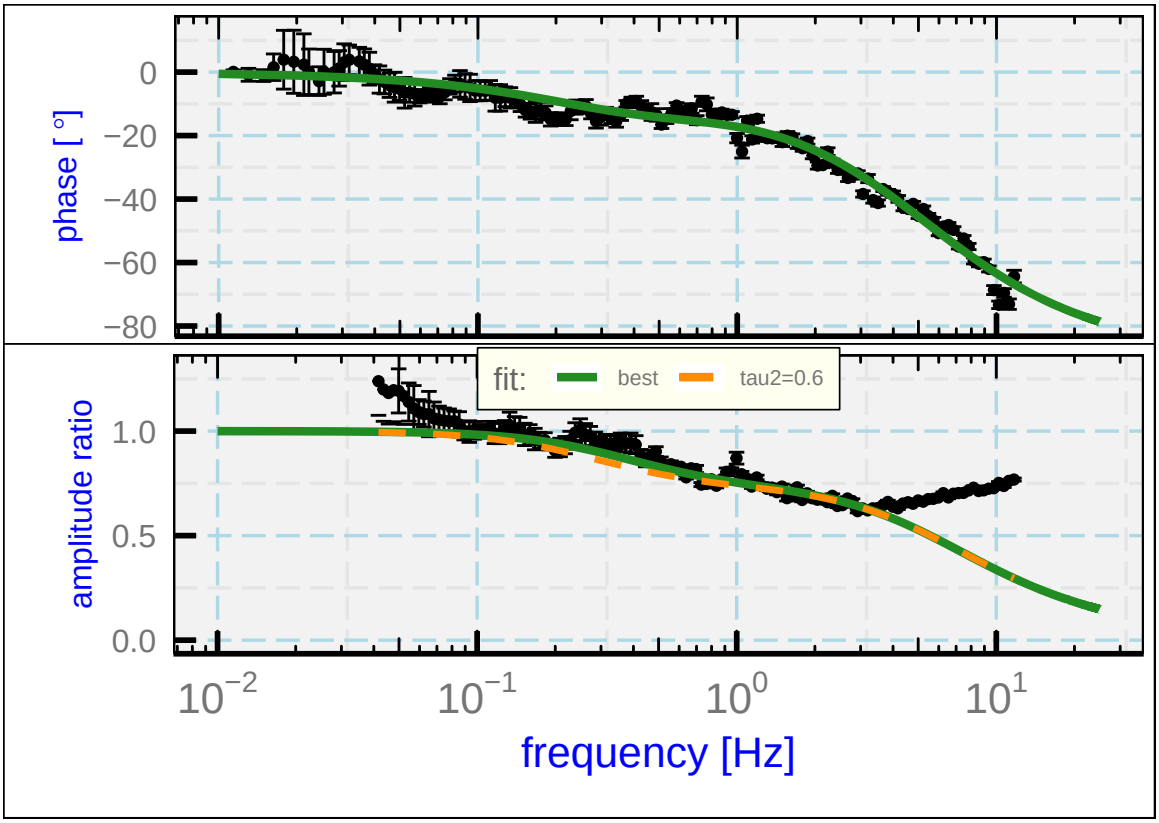

Figure 2: (top): Phase of measured recovery temperature relative to dynamic heating, for the measurements (with error bars) and for the theoretical response for the best-fit parameters (green line). The error bars indicate two-standard-deviation ranges in the mean at each plotted point. Data from the flight segments listed in Table 1.
(bottom): The ratio of the spectral amplitude for the measurement of recovery temperature ($T_m(t)$) to that for dynamic heating (Q), shown as the plotted data points. There are additional data points at frequencies below about 0.04 Hz that do not appear in this plot because they lie above the upper limit for the ordinate. The green line is the prediction from the transfer function determined from the best-fit values matching the phase lag between these variables, and the dashed orange line is a similar result with the second time constant τ_2 increased from 0.447 to 0.6 s to illustrate sensitivity to this parameter.

The fit procedure used (7) and (8) to find the theoretical value of the amplitude ratio and phase at each frequency represented in the observations. For assumed values of the three parameters a, τ_1 and τ_2, a chi-square was calculated from the differences between these theoretical values and the observed values. The frequencies used for the fit were 0.01 to 12 Hz for the measurements of phase and 0.1 to 3 Hz for the measurements of amplitude ratio, to avoid regions where effects other than dynamic heating appear to bias the measurements. Then a search procedure varied these parameters to seek the minimum value of the chi-square.[4] The resulting values were $a = 0.73$, $\tau_1 = 0.031$ and $\tau_2 = 0.45$. The chi-square for the fit is about 18 times larger than expected if the fit represents the measurements to measurement uncertainty, so it is difficult to assign uncertainty limits to this result on the basis of this fit because of this not-understood excess chi-square, but the fit minimum distinguished nearby values to about three significant digits in all three parameters. The Hessian from the fit implies that the results with standard uncertainties are $a = 0.733 \pm 0.004$, $\tau_1 = 0.0308 \pm 3 \times 10^{-4}$ and $\tau_2 = 0.45 \pm 0.02$.

To complete the iteration discussed earlier, the measured recovery temperature was then corrected via method 1 from Appendix A, using the parameters from this first fit, to find a prediction for the actual recovery temperature $T_r(t)$. After recalculating Q using (9) with that estimate of $T_r(t)$ in place of $T_m(t)$, the calculation of phase and amplitude was repeated and the results were fitted again by adjusting the fit parameters. Only very minor changes arose from this procedure even after one iteration, but the iterated result is the one used here to represent the unheated Rosemount 102E4AL sensor.

The airflow and typical flow angles approaching a sensor can affect its response, so the results might change when installed on a different location or a different aircraft. Therefore a similar evaluation examined the response of this same sensor when flown on the NSF/NCAR GV, which flies significantly faster than the C-130. The results of a study using a combined low-level dataset from the SOCRATES (McFarquhar et al. [2014]) and CSET (Albrecht et al. [2019]) experiments, which were flown over the Pacific Ocean, were similar to but slightly different from the coefficients determined on the C-130, with both time constants a little smaller than found for the C-130 (τ_1 =0.024 and τ_2 =0.22). This might be expected at greater airspeed, as discussed in Sect. 2.4.3.

2.4.2 Heated sensors

Measurements from two slower sensors, a heated Goodrich/Rosemount 102 sensor and a similar "Harco Model 100009-1 Deiced TAT" (HARCO) sensor, have also been evaluated, but only the latter is discussed here because they have similar response. The spectral variance for both these measurements has apparent rapid attenuation beginning at about 0.1 Hz, as shown in Fig. 3, and the response is attenuated seriously above about 1 Hz.

Attempts to use the same three-parameter representation of the transfer function relative to dynamic heating led to unsatisfactory fits, so a different approach is used here. Because the evaluation in Sect. 2.4.1 provides a good representation of the unheated Rosemount 102E4AL sensor, the measurements from that sensor, corrected as will be described in Appendix A, were used

[4]The code can be found in the "Rnw" document that generates the present document. It used the "optim()" function from the R "stats" package produced by the R Core Team [2019].

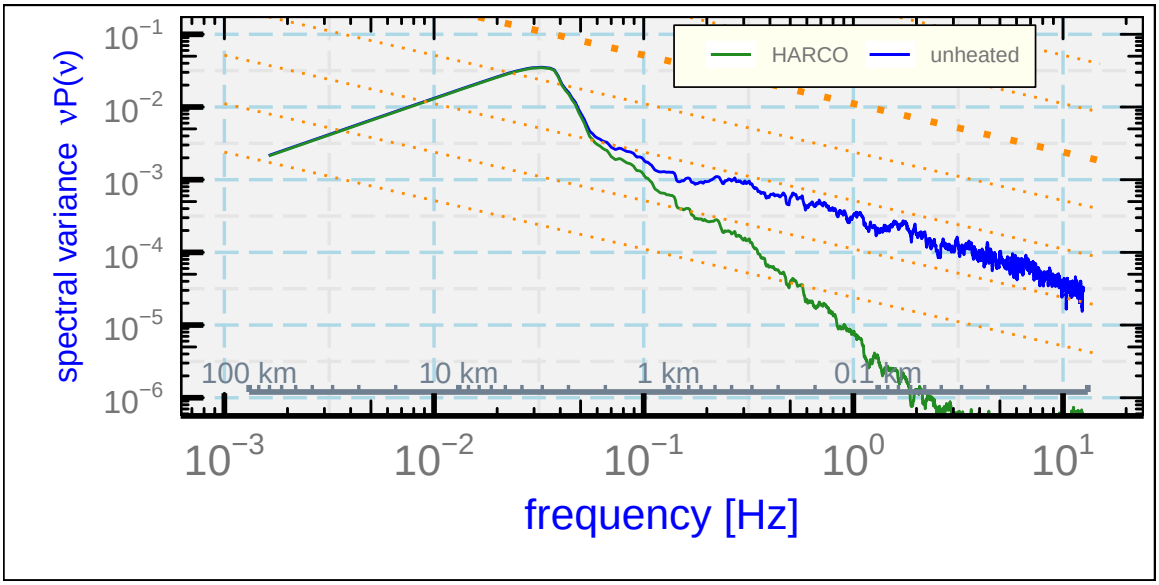

Figure 3: Spectral variance $P(\nu)$ weighted by frequency (ν) for the recovery temperature measured by a heated HARCO and an unheated Rosemount sensor.

as the reference for the assumed-correct recovery temperature. Then the phase and amplitude ratio were found for the transfer function required to produce the heated-probe measurements from the unheated-probe measurements. This did not require any assumptions about equations or parameters determining the transfer function.

To characterize the response of the heated HARCO sensor, boundary-layer flight segments from the SOCRATES and CSET projects (referenced earlier in connection with the unheated probe) were compiled into one data set from the flight periods shown in Table 2. An unheated Rosemount 102E4AL sensor was also onboard, so corrected measurements from that sensor were used as the reference against which to determine the gain and phase of the transfer function.

Project / Flight	**start [UTC]**	**end [UTC]**
CSET / 5	2015-07-14 17:52:00	18:02:00
CSET / 5	2015-07-14 19:45:30	19:55:30
CSET / 5	2015-07-14 20:37:17	20:47:17
SOCRATES / 15	2018-02-24 5:52:00	6:02:00
SOCRATES / 15	2018-02-24 6:05:00	6:15:00

Table 2: Flight segments used to determine the response characteristics of a heated HARCO sensor.

The measured phase and amplitude ratio for this data set are shown in Fig. 4. The fits for the response function defined by (7) and (8) are shown as the blue lines labeled "3-par" in that figure. The fitted values for $\{a, \tau_1, \tau_2\}$ were $\{0, 0.05, 1.12\}$, and to obtain this result the fit had to be constrained to keep a non-negative. A value of zero for the parameter a would indicate that no heat is transferred from the sensing wire to the air, but instead all is transferred to the support which has a relatively slow characteristic response.

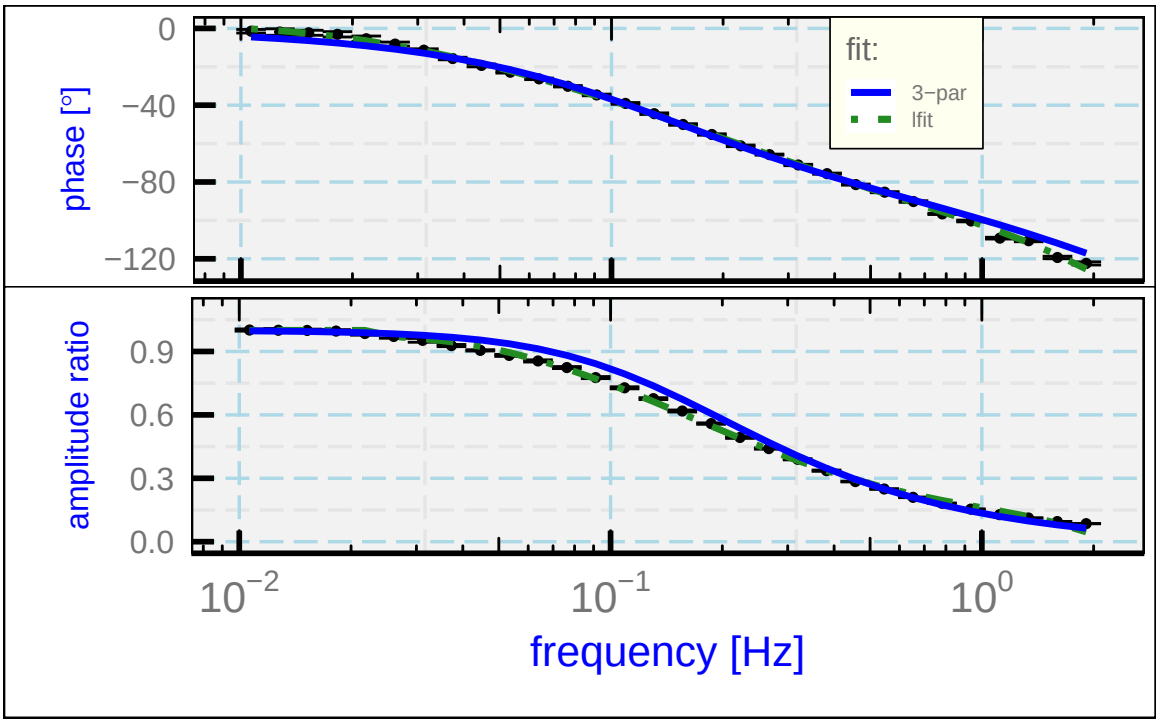

Figure 4: The phase (top) and gain (bottom) for the transfer function characterizing a heated HARCO temperature sensor. The measurements are indicated by error bars that show two-standard-deviation limits from the mean value). Two fits to the measurements, one based on the three-parameter representation ("3-par") and one on a polynomial fit ("lfit"), are described in the text.

The three-parameter fit is not consistent with the measurement errors even though it provides an approximate representation of the transfer function. The apparent reason is that there is conflict between the constraints imposed by the amplitude ratio and the phase, such that either could be represented reasonably but not both. The actual transfer function has some complex features, including frequencies where the phase shift reaches values below $-90°$ (not possible for a simple exponential time response) and values of the phase shift of about $-38°$ at 0.1 Hz where the amplitude ratio is still high (about 0.75). The amplitude decreases to e^{-1} at about 0.34 Hz, as would be the case for a first-order time constant of about 1.3 s, so this could be considered another measure of the response. However, that value does not extrapolate well to other frequencies and the phase shift at 0.34 Hz is approximately $-73°$, which would indicate that the measurement of a real contribution to sensible-heat flux at this frequency would be only about 10% of the correct value.

Because the three-parameter fit distorted the measured result, fits in the logarithm of the frequency were used to provide a better representation of the measurements, as shown by the dashed green lines labeled "lfit". Those fits are given by these equations and coefficients, with $x = \log_e(\nu/\nu_0)$ where ν is the frequency, $\omega = 2\pi\nu$ and $\nu_0 = 1\,\mathrm{Hz}$:

$$\text{for } \nu > 0.024\,\mathrm{Hz},\ H(\omega) = (h_0 + h_1 x + h_2 x^3 + h_3 x^4 + h_4 x^5) e^{i\phi(\omega)} \tag{12}$$

$$\text{for } \nu \le 0.024\,\mathrm{Hz}, \quad H(\omega) = 1$$

$$\phi(\omega) = p_0 + p_1 x + p_2 x^2 + p_3 \arctan(\nu/\nu_0)$$

The coefficients obtained by fitting to the observations are h_{0-4} ={0.161, −0.136, −0.0760, −0.0309, −0.00324} and p_{0-3} ={−155.2, −62.8, −6.35, 67.2}. This fit can be used to represent the transfer function better than the three-parameter fit (with negative-frequency values defined as the complex conjugate of the values at the corresponding positive frequency), although the fit needs to be modified above about 2 Hz because those values were not constrained by the measurements. A suggested modification is to duplicate the value at 2 Hz to higher frequencies; this appears to be adequate because there is so little variance measured by this sensor at these frequencies, but it is important to avoid possible zeroes that otherwise arise from extrapolation.

2.4.3 Expected dependence on flight conditions

Based on measurements in a wind tunnel, Stickney et al. [1994] indicated that the fast-response characteristic time τ_1 for the unheated Rosemount 102E4AL sensor varies approximately as $\log(Z^{-0.6})$ where $Z = M\rho_a/\rho_s$ with M the Mach number, ρ_a the air density and ρ_0 the air density under standard conditions. The mean value of Z for the flight segments used to find the best-fit parameters was $Z = 0.3$, so this suggests that the first characteristic time for that sensor is best represented by

$$\tau_1'(Z) = \tau_1 \left(\frac{0.3}{Z}\right)^{0.6} . \tag{13}$$

There is no similar evidence for τ_2, but it might be expected to have similar dependence because this is approximately the Reynolds number dependence and the Nusselt number characterizing ventilated heat transfer often is represented by a power-law relationship to the Reynolds number. If both heat transfer terms scale similarly, it might be expected that a will be unchanged.

For these reasons, the time parameters obtained in preceding sections have been adjusted to a reference value of $Z = 0.3$ in Table 3. For other conditions, it is suggested that the best estimate will be to multiply τ_1 and τ_2 by $(0.3/Z)^{0.6}$. (Having these parameters vary is in conflict with the "LTI" assumption leading to the transfer function, but these variations are minor over short times so incorporating this variation should produce reasonable results.)

sensor	a	τ_1 [s]	τ_2 [s]
unheated Rosemount 102E4ALon C-130	0.73	0.031	0.45
unheated Rosemount 102E4AL on GV	0.65	0.024	0.22
heated HARCO	0.0	0.058	1.29

Table 3: Parameters for the time response of available temperature sensors on the NSF/NCAR aircraft, adjusted to $Z = 0.3$. For other conditions, scale as represented for τ_1' in (13).

2.5 Response to a step change

Previous studies have mostly used sharp temperature changes in the atmosphere, for example from climbs through the inversion at the top of a boundary layer, to study the time response. A search of representative VOCALS climbs and descents through inversions capping the marine boundary layer found that almost all have measurable structure and are not discrete transitions, but there was one near-ideal example. Figure 5 shows the time history of the measured temperature for 8 s from VOCALS flight 3, starting at 8:13:50 UTC, when the aircraft descended through the top of the marine boundary layer at approximately 1000 ft/min (around 5 m/s). The temperature structure in this case was remarkably consistent with a near-constant temperature above the inversion and a near-adiabatic temperature structure below the inversion.

The suggested measurand history, if the discontinuity at the inversion is discrete, is that shown by the dashed black and dashed red lines.. The predicted time response from (4) for assumed time constants for the unheated Rosemount 102E4AL sensor adjusted for air density and flight speed is shown as the magenta line in Fig. 5. The predicted response is consistent with the observations and supports the approximate validity of the parameters determined from fits to the response to dynamic heating.

2.6 Uses of the transfer functions

The transfer functions have two potential uses: (i) to predict how airborne thermometers will respond; and (ii) to correct measurements to compensate for the time response of the sensors.

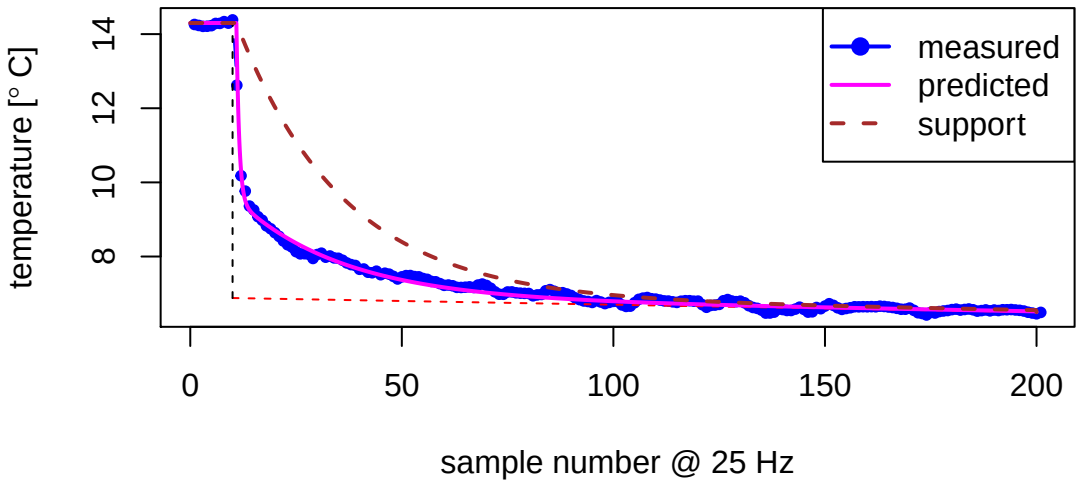

Figure 5: (blue dots): Temperature measured at 25 Hz during descent through an inversion capping the marine boundary layer, from VOCALS flight 3, starting at 8:13:50 UTC. The descent rate was approximately 5 m/s. The dashed red line shows a dry-adiabatic lapse rate in the marine boundary layer, and the dashed black line is a reference line indicating the location of the top of the boundary layer.The prediction using the parameters listed in the text is shown as the magenta line, mostly over the blue dots representing the measurements. The dashed brown line is the calculated temperature of the support that contacts the sensing wire.

The two sections that follow are examples of these two uses. In the next section, the transfer functions are used to assess how sensors respond to dynamic heating and to develop appropriate correction schemes. Then the following section applies the transfer functions to improve measurements of the flux of sensible heat.

The preceding discussion has focused on the recovery temperature that is the measurand, as expressed by (10), because the sensor responds to that temperature. Corrections should be made to the measurement of the recovery temperature, here represented by T_m, to obtain an improved estimate of the measurand. It is an error to apply the corrections to the air temperature after correction for dynamic heating (as in, e.g., McCarthy [1973], Inverarity [2000], Nicholls [1978] and others) because then the correction is applied also to the dynamic-heating term to which it does not apply. This will introduce noise into the calculated air temperature if the sensor cannot respond fully to fluctuations in dynamic heating.

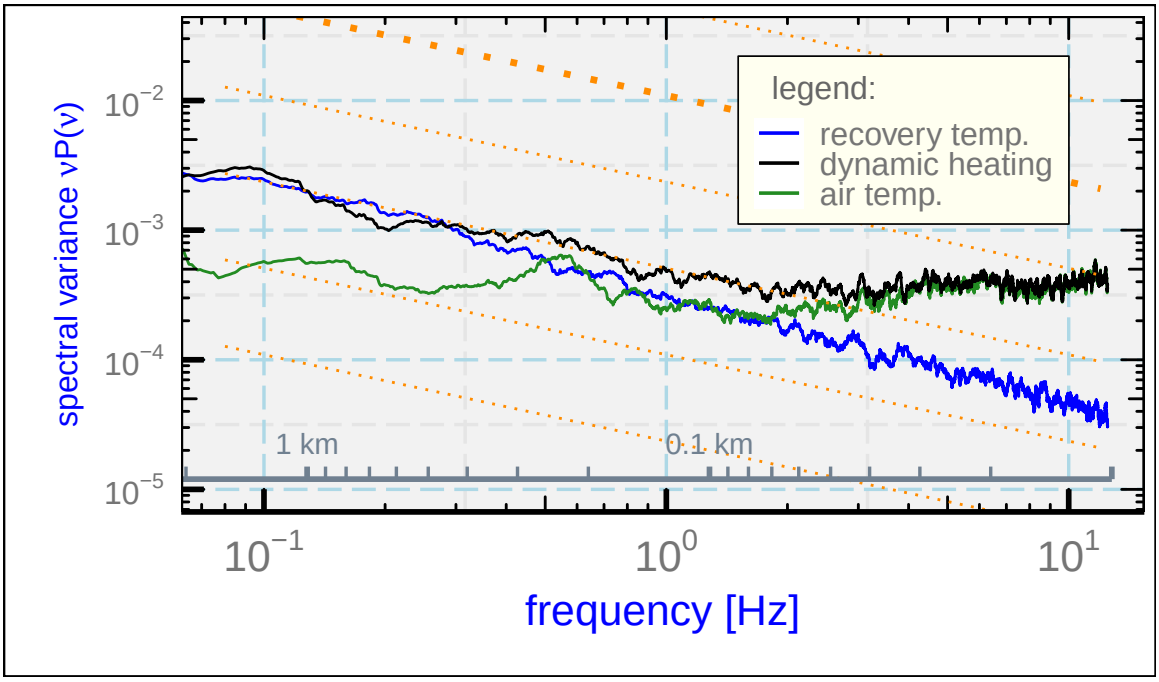

Figure 6: The weighted variance spectrum as a function of frequency ν for the recovery temperature measured by a Rosemount 102E4AL sensor. The spectra for the dynamic-heating term and for the calculated air temperature after this correction is applied are also shown.

3 Correcting for Dynamic Heating

Airborne thermometers sense the recovery temperature produced when air is compressed as it enters the housing. Data-processing algorithms used to produce data archives from most airborne measurement platforms subtract an independent estimate of dynamic heating to obtain a resulting measurement of the ambient air temperature. The dynamic-heating term can exceed 20°C at jet-aircraft flight speeds, so the correction is large and fluctuations in this term are often the dominant source of variations in the recovery temperature. As described in Sect. 2.2, when the sensor cannot respond to fluctuations in dynamic heating, this procedure introduces errors and excess noise into the resulting air temperature. A modified correction procedure is proposed here that instead corrects for dynamic heating only after filtering to match the response of the temperature sensor. This removes a significant source of error present in many temperature measurements made from research aircraft.

Figure 6 illustrates the problem. The measurements are from a low-level flight segment over the ocean where other indications are reasonably consistent with an inertial sub-range. The slope of the temperature variance spectrum would be expected to be -5/3 (or -2/3 in this plot where the spectrum is weighted by the frequency). The variance spectrum of the measured recovery temperature has a steeper slope than this but that would be expected if the time response attenuates the signal at higher frequencies. However, the variance spectrum for the estimated ambient temperature appears to have a substantial amount of high-frequency contamination. This matches the high-frequency portion of the spectrum for dynamic heating. If the sensor measured the correct recovery temperature its spectrum should exceed that of the ambient temperature, as is

the case around 0.1 to 0.5 Hz, so that the subtraction of dynamic heating would produce smaller variance in the measured ambient temperature. Later figures (Figs. 10a and 10b) will show anecdotal examples of the errors introduced by the conventional correction.

Data processing should instead apply a correction that represents how dynamic heating affects the sensor, and that correction should not include fluctuations at frequencies to which the sensor does not respond. The approach followed in this paper is therefore to use the transfer function to characterize the response of an airborne temperature sensor to dynamic heating so that only that response is subtracted from the measurement. This is made possible by the assumed linearity in response of the sensor, which is required if this part of the response is to be separated from the more general response to the combination of dynamic heating and true fluctuations in temperature.

The transfer function shown in Fig. 1 indicates that the response to fluctuations at 5 Hz is only about 50% of the imposed amplitude, and at 10 Hz the response is only about 35%. Furthermore, the phase at 10 Hz is shifted by about 62°. Using the measurement of dynamic heating Q as specified by (9) to correct the measured recovery temperature will therefore over-correct and produce erroneous fluctuations in the measured air temperature unless Q is filtered to represent the sensor response..

A revised dynamic-heating adjustment filtered to represent how the sensor will respond is denoted Q'. When no correction is applied to the measured recovery temperature $T_m(t)$, the ambient temperature T_a should be estimated from

$$T_a(t) = T_m(t) - Q'(t) \tag{14}$$

instead of (10). The appropriate correction can be obtained from the transfer function in several ways, as discussed next.

3.1 A filter for dynamic heating

The impulse response of the sensor can be found from the inverse Fourier transform of the transfer function. Once that is determined, appropriate moving-average coefficients can be found from the impulse response, and those coefficients define a digital filter that represents the sensor response. The procedure used here is somewhat arbitrary and a better filter could probably be designed, but this functions reasonably for 25 Hz measurements. Details including the filter coefficients are provided in Appendix B.

Figure 7a shows the impulse function for the unheated Rosemount and heated HARCO sensors, and Fig. 7b shows corresponding moving-average coefficients for a filter obtained from this impulse function. There is significant ringing in the filter for the Rosemount sensor because the shorter time constant for the sensor, 0.03 s, is smaller than the time between 25-Hz samples. The impulse response for the slower HARCO sensor leads to a much broader impulse response function. Both sets of moving-average coefficients sum to more than 0.99 as calculated but were then normalized to sum to 1.0.

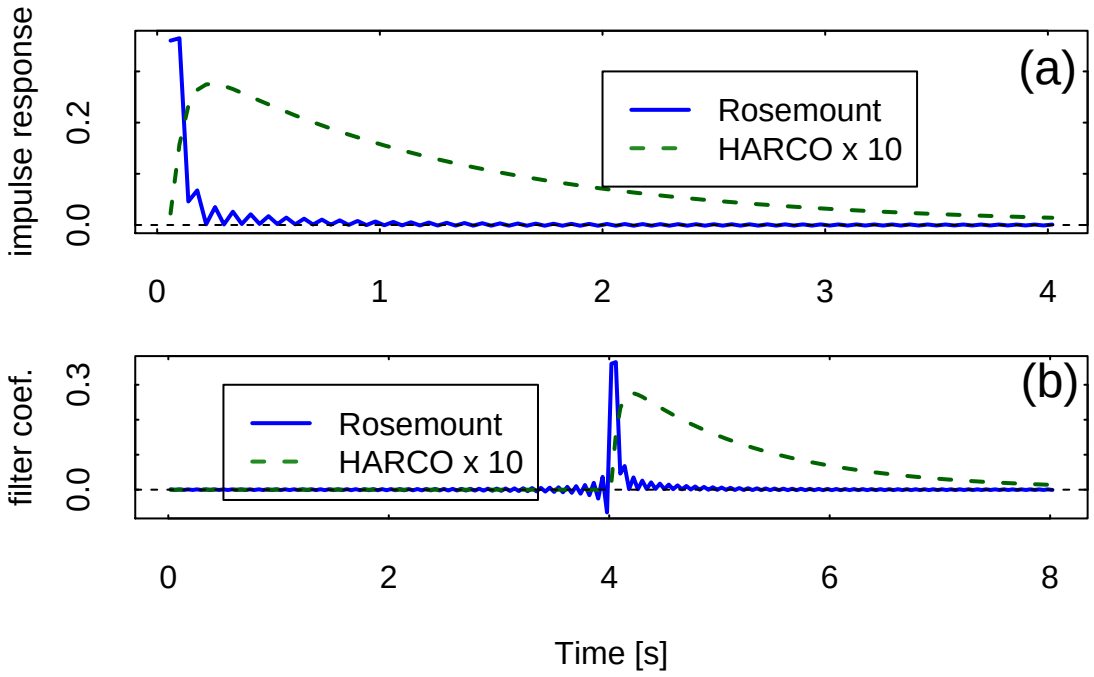

Figure 7: (a) The impulse response function found from the inverse Fourier transform of the transfer function for the unheated Rosemount 102E4AL sensor (Rosemount) and for the heated HARCO sensor (HARCO), using the response parameters from Table 2 of Part 1. The impulse response for the HARCO sensor is multiplied by 10. (b) A filter function (moving-average coefficients spanning 8 s) obtained from the impulse response function. The filtered result must be shifted forward in time by 4 s to compensate for the delay introduced by the filter. The coefficients are multiplied by 10 for the HARCO sensor.

3.2 Other filtering methods

Two other calculations can produce the appropriately filtered response to dynamic heating $Q'(t)$:

1. Section 2 showed that the transfer function is represented reasonably by the solution to two coupled differential equations. Numerical integration of those equations can then produce the predicted response of the sensor to dynamic heating. The equations from Sect. 2.1, revised to apply to dynamic heating, are these:

$$\frac{dQ_{qs}(t)}{dt} = \frac{Q(t) - Q_{qs}(t)}{\tau_2} \tag{15}$$

$$\frac{dQ'(t)}{dt} = \frac{\{aQ(t) + (1-a)Q_{qs}(t)\} - Q'(t)}{\tau_1} \tag{16}$$

   where the first equation describes the effect of dynamic heating on the support structure of the temperature sensor, leading to support-structure variations in temperature of $Q_{qs}(t)$. and the second describes the response of the sensing wire to the combined effects of this influence on the support temperature and the dynamic-heating term. This separation relies on the linearity of the underlying equations, which makes it possible to represent the effect of dynamic heating in isolation from real fluctuations in temperature. Euler integration of these differential equations led to erroneous results at high frequency arising from inadequate resolution in the integration, so a fourth-order Runge-Kutta integration[5] was used instead.

2. The response specified by the frequency-domain transfer function $H(\nu)$ can be realized by Fourier transforms, by first calculating the Fourier transform of the dynamic-heating signal (here denoted $\hat{Q}(\nu) = \mathscr{F}(Q(t))$ where $\mathscr{F}$ denotes the Fourier transform) and then using the inverse Fourier transform ($\mathscr{F}^{-1}$) to estimate the sensor response:

$$Q'(t) = \mathscr{F}^{-1}(H(\nu)\hat{Q}(\nu))$$

Figure 8a shows the variance spectra that result from all three methods when applied to measurements from an unheated Rosemount 102E4AL sensor. The modified variance spectrum obtained by integration of the underlying differential equations is shown as the orange line ("DiffEq") in Fig. 8a. The dynamic-heating correction is appropriately attenuated at high frequency after this integration. The results obtained after filtering as described in the Sect. 3.1, labeled "filter", or after Fourier transformation, labeled "FFT", are overlapping so as to be indistinguishable in this plot. These corrected estimates of the dynamic heating are attenuated even more than the result from numerical integration and are in better agreement with the predicted effect of the transfer function, which for example predicts attenuation of the variance spectrum by a factor of 0.096 for the component with frequency 10 Hz. The numerical integration was closer to the results of

[5]The integration method was fourth-order Runge-Kutta with adjustment of the time step to control the estimated tolerance during the integration. The method was based on Cash and Karp [1990]. The integration was also tested with the R routine "rmutil::runge.kutta" Swihart and Lindsey [2019]. See the Workflow document for additional details.

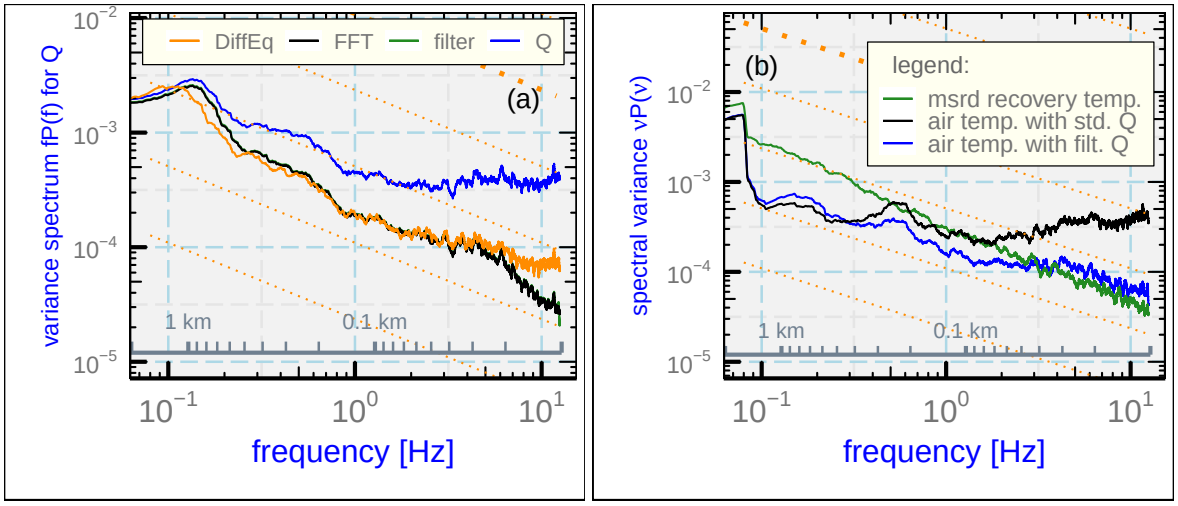

Figure 8: Variance spectra for the unheated Rosemount 102E4AL sensor, for the same flight segment used for Fig. 6.
Left, (a): The dynamic-heating term ("Q:) and for the filtered term obtained by integrating the differential equations for the derivatives ("DiffEq"), by Fourier transformation with application of the transfer function ("FFT"), or applying the digital filter ("filter"). The result for the latter is so close to that for "FFT" that it is obscured in this plot.
Right, (b): The measurement of recovery temperature and ambient temperature calculated using the filtered dynamic-heating term. The original variable for ambient temperature based on standard processing is also shown.

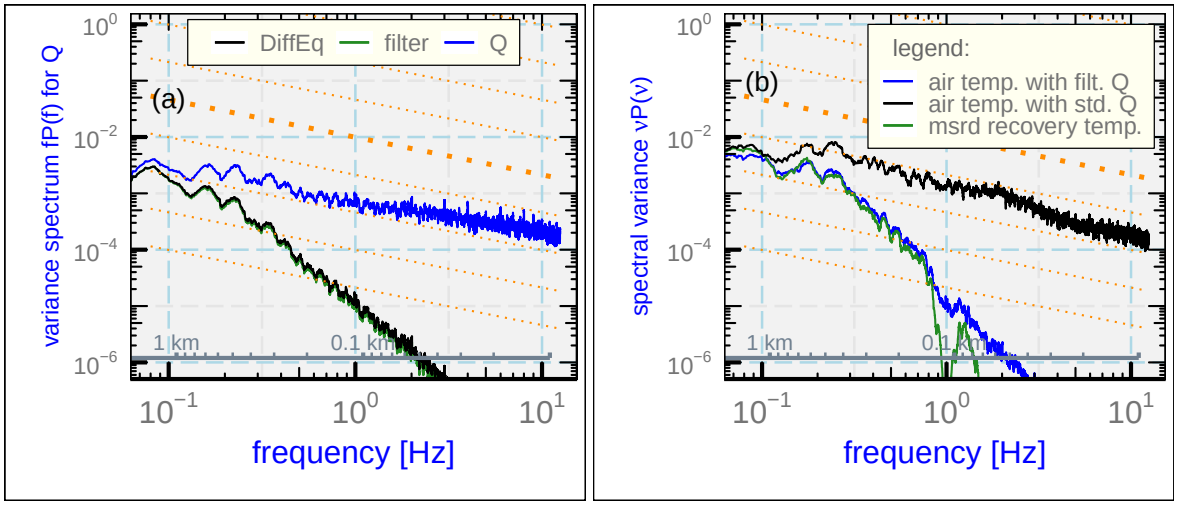

Figure 9: Variance spectra for the heated HARCO sensor.
Left, (a): The unmodified dynamic-heating term ("Q") and the two filtered terms. The results from solving the differential equations ("DiffEq") or from application of the digital filter ("filter") are overlapping and indistiguishable in this figure.
Right, (b): The temperature as modified by filtering the dynamic-heating term (blue line). The other plotted spectra are for the measured recovery temperature and the air temperature with the conventional dynamic-heating correction.

the filter if the measurements are interpolated to 125 Hz with 25-Hz smoothing, integrated, and then resampled to obtain 25 Hz measurements. This iondicated that the discrepancy in results is attributable to accumulating numerical errors in the integration, but the integration became awkwardly slow when performed at 125-Hz resolution. The equivalence of the results from the digital filter and from Fourier transformation with application of the transfer function supports the validity of these results and suggests that these are preferable and equivalent methods for filtering dynamic heating to match the response of the temperature sensor.

A revised estimate of the ambient air temperature was calculated using (14) and the corrected dynamic-heating term Q'. The spectral variance for this air temperature, shown in Fig. 8b as the blue line, is improved considerably at high frequency vs. that using the standard correction.

In the case of the heated sensors, the revision is still more significant because they respond more slowly. Figure 9a shows the result of filtering the dynamic-heating term for a heated HARCO sensor. The result of integration ("DiffEq") and the digital filter ("filter") are almost identical so there is no evidence of the numerical problems that were encountered with the integration for the unheated Rosemount sensor. The difference vs. the original is quite dramatic even at 1 Hz, and the errors are significant for all frequencies above about 0.1 Hz. Because either corrected variance spectrum represents how the temperature sensor responds to the actual fluctuations, subtracting the actual fluctuations in dynamic heating instead of the filtered fluctuations introduces substantial erroneous variability into the calculated air temperature.

Figure 9b shows how this affects the spectral variance of the measured air temperature. The slow response of this sensor causes the measured recovery temperature (green line) to have very low spectral variance when the frequency is above 1 Hz, so the variance in the standard

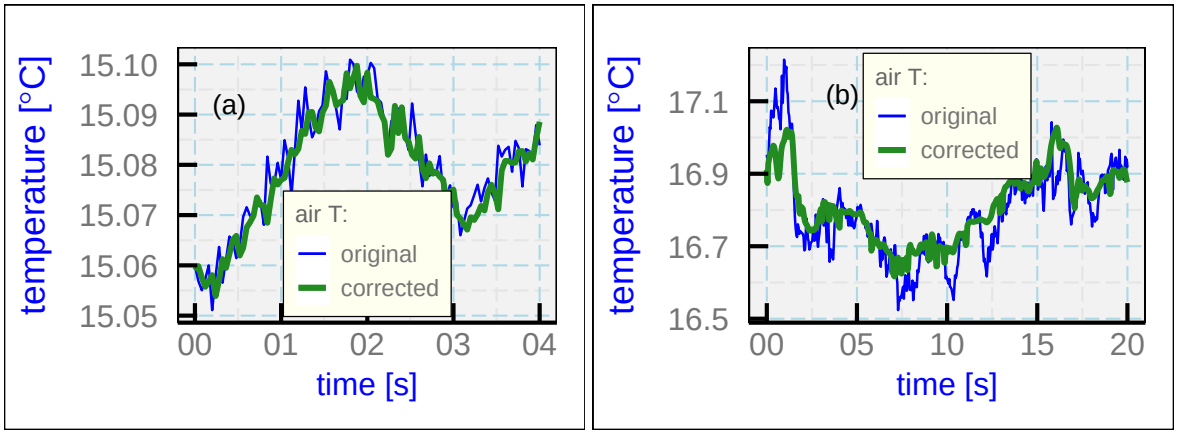

Figure 10: Comparison of the original measured temperature and the same temperature after filtering the dynamic-heating correction:
(left): An unheated Rosemount 102E4AL sensor; (right): A heated HARCO sensor.

air-temperature measurement in this frequency range is almost entirely caused by erroneous adjustment for fluctuations in dynamic heating to which the sensor does not respond. The correction procedure using a filtered dynamic-heating correction removes this excess spectral variance and produces a signal where the variance for frequencies above about 0.1 Hz arises primarily from variance in the measured recovery temperature. The variance spectrum for the conventionally processed temperature looks approximately as might be expected in an inertial subrange, but the variance above about 0.5 Hz is a false signal that does not arise from real variance in temperature. It therefore becomes very important to use this revised processing scheme to avoid erroneous measurements even for changes occurring over 5 s or more. The reasonable appearance of the variance spectrum for the standard result is misleading because the measurement is not responding to real fluctuations in air temperature at high frequency. The measurement with filtered dynamic heating is a better indication of the measured fluctuations.

For the unheated Rosemount 102E4AL sensor, Fig. 10a illustrates the removal of erroneous structure by filtering, and Fig. 10b shows a similar example for the heated HARCO sensor. These examples illustrate that the erroneous fluctuations in the uncorrected measurements can be important in many potential uses of these measurements and should be removed as part of standard processing. The effect is particularly significant for the HARCO sensor, for which there are large fluctuations in Fig. 10b that are caused by fluctuations in dynamic heating to which the sensor does not respond. [6]

[6]For the NSF/NCAR GV, the dynamic-heating term is complicated further by resonance in the pressure lines connecting the transducers to the pressure sources. This is discussed in detail in Appendix B.

4 The Flux of Sensible Heat

4.1 Outline of the correction procedure

The measured air temperature T_a is normally calculated by subtracting a dynamic-heating correction Q from the measurement: $T_a = T_m - Q$ where T_m is the measured recovery temperature. However, here it is desired to correct the resulting measurement on the basis of a known transfer function $H(\nu)$ that describes how the sensor responds to the input. That input (the measurand) is the recovery temperature $T_r = T_a + Q$, which differs from the measurement T_m when the sensor output lags behind the input. The correction procedure therefore should correct the measurement T_m to obtain an improved estimate of the recovery temperature and then use that corrected estimate of the recovery temperature to find the air temperature.

Most past studies of temperature corrections (e.g., McCarthy [1973], Nicholls [1978], Inverarity [2000]) applied corrections instead to the air temperature after correction for dynamic heating. That applies the full correction for dynamic heating Q without considering that the sensor may respond only partly to high-frequency fluctuations in Q, which was shown in Part 2 to lead to erroneous noise in the air temperature. Then that noise is amplified by the correction procedure. These errors are avoided if corrections are applied instead to the measurement of the recovery temperature. Then the appropriate amplification of signals restores the fluctuations produced by dynamic heating and those fluctuations are appropriately removed by subtracting the measured dynamic heating term from the corrected recovery temperature.

The procedure used here is as follows:

1. Find the transfer function, as in Sect. 2. This is best done for the conditions, sensor, and aircraft that collect the measurements to be used for the flux measurement.

2. Find the air temperature or, equivalently, the Fourier representation of the air temperature. In terms of Fourier transforms, denoted here by the symbol "^", $\hat{T}_m(\nu) = H(\nu)\hat{T}_r(\nu)$ so the value of the recovery temperature can be estimated from the inverse Fourier transform of $\hat{T}_m(\nu)/H(\nu)$. The best estimate of the Fourier representation of the air temperature is then obtained from $\hat{T}_a = \hat{T}_m(\nu)/H(\nu) - \hat{Q}(\nu)$. This Fourier representation of the air temperature can be multiplied by the complex conjugate of the Fourier representation of the updraft to yield the cospectrum representing the flux of sensible heat, with an appropriate scale factor as specified in (**??**).[7]

3. Calculate the cumulative cospectrum for the cross-spectrum of temperature and updraft, with a choice made regarding which frequency interval to include. This will normally exclude wavelengths longer than a few kilometers.

4. Calculate the flux from the sum of the resulting cospectrum over an appropriate frequency interval.

[7] The corrected recovery temperature also can be calculated by integrating the equations presented in Sect. 2.1.

4.2 Examples of Measured Cospectra and Fluxes

Two examples of measured cospectra illustrate the effect of the correction. The first example is from the "Southern Ocean Clouds, Radiation, Aerosol Transport Experimental Study" (SOCRATES) (flight 15, 24 January 2018, 6:00:00 to 6:15:00 UTC) and the second is from the "Cloud Systems Evolution in the Trades" (CSET) experiment (flight 5, 14 July 2015, various segments from 17:50:00 to 20:50:00 UTC). The flight segments that were used were all at low level (150 m) in the marine boundary layer over Pacific Ocean. An unheated Rosemount 102E4AL sensor was used on the NSF/NCAR GV during these projects. In each case, the cospectra from three flight segments of 5 min (SOCRATES) or 10 min (CSET) duration were averaged to produce the measured cospectra. The flux estimates were then compared without correction and corrected using the appropriate transfer function as determined in Part 1.

The results are shown in Figs. 11, where the measured fluxes of sensible heat are listed in the plot titles. This plot format is unconventional so some explanation is provided below because this plot will be used throughout the paper as the primary display of the cospectrum. The cospectrum can be positive or negative, so it is usually plotted using a linear scale for the abscissa. However, as the figure shows, the range of ordinate values is displayed better with a logarithmic scale, even after weighting the cospectrum by frequency. The compromise made in this plot is to use a logarithmic scale but plot negative values with sign reversed and with a different color, here red instead of blue. The values plotted in red therefore should be regarded as negative values of the plotted magnitude. There is then a dead-band at the bottom of the plot where spectral values with very small absolute value lie, here absolute values smaller than $10^{-2}\,\mathrm{W\,m^{-2}}$. Weighting by frequency is used as is appropriate for a logarithmic abscissa. Other features of this plot and computation conventions include the following:

1. The cospectrum (blue line) has been smoothed using Daniell smoothing, with consecutive smoothing using width-3 for frequencies above 0.01 Hz, then width-5 for frequencies above 0.1 Hz, then width-17 for frequencies above 1 Hz. For these 5-min flight legs and for 25 Hz measurements, the maximum smoothing interval corresponds to a smoother spanning about 0.05 Hz, so most spectral features are retained even with this strong smoothing. Additional smoothing results from averaging three cospectra to obtain the plotted values.

2. Further smoothing is included by binning the results into 100 logarithmically spaced intervals in frequency and averaging in those bins. That results in the blue dots (or dark red dots for negative points).

3. A shaded ribbon denotes the standard deviation of the values in the bins. In many cases it is too narrow to be visible.

4. The total flux indicated in the title is that arising from the part of the flux with frequency above 0.01 Hz. This corresponds to a wavelength of more than 10 km. In addition, there is another estimate of the contribution to the flux from wavelengths below a selected limit, here 2 km. That or a still smaller wavelength limit is often a reasonable estimate of the part of the flux contributed by turbulent air motions in the boundary layer, so that will be regarded as the primary measurement of sensible-heat flux.

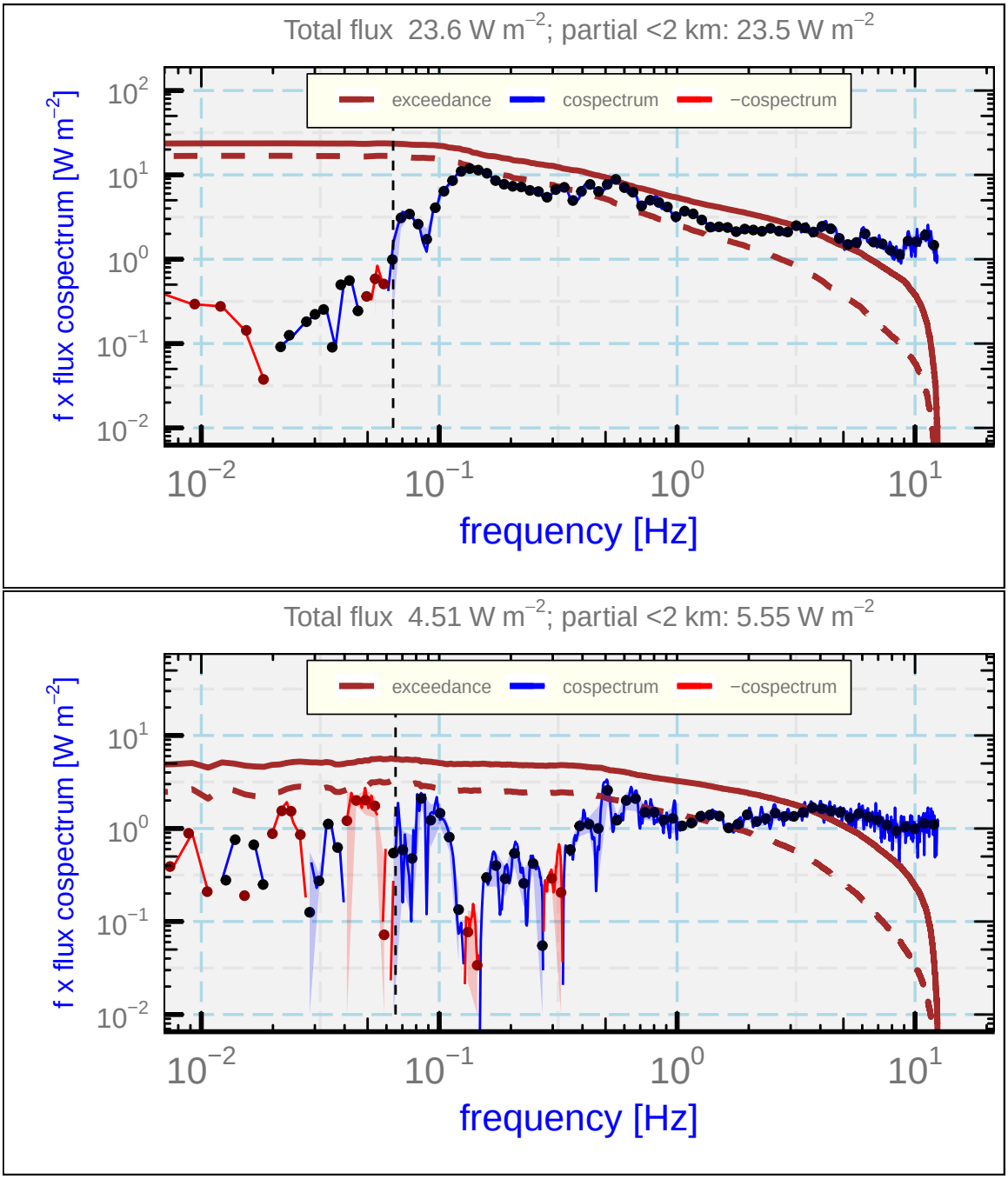

Figure 11: (top): The corrected flux of sensible heat for SOCRATES flight 15, 6:00:00 to 6:15:00, a low-level flight segment over the southern-hemisphere ocean. The "exceedance" is the complement of the cumulative distribution function (i.e., the sum of contributions from frequencies above the plotted value), and the dashed brown exceedance line is that without transfer-function correction but with adjustment of the dynamic-heating term to incorporate the estimated response of the temperature sensor.
(bottom): Cospectrum for the flux of sensible heat, for three 10-min flight segments from the CSET project. The dashed brown line is the exceedance distribution before correction, which gives a flux of 3.07 W m${-2}$ for wavelengths smaller than 2 km and 2.06 W m^{-2} for frequencies above 0.01 Hz.

5. One additional line is plotted brown and labeled "exceedance." That is a cumulative distribution function for the cospectrum, called "exceedance" because it is the contribution from all frequencies *higher* than the indicated value. At high frequency on a logarithmic scale, where some of the most interesting variation is located, that is more informative that the conventional cumulative distribution. The units for exceedance are $\mathrm{W\,m^{-2}}$, not $\mathrm{W\,m^{-2}}$ per logarithmic interval as is the case for the weighted cospectrum.[8]

The exceedance distributions before correction, shown as the dashed brown lines, were calculated using a dynamic-heating correction that was filtered to match the response of the sensor, but otherwise was not corrected. In the two cases, without correction for the response as represented by the transfer function, about 30% and 44% of the flux, for the SOCRATES and CSET cases respectively, would be missed. The underestimation is particularly serious at higher frequencies: In both cases the measured contribution from frequencies above 1 Hz is about twice as large after correction as it is without correction.

Lawson and Rodi [1992] estimated that, in comparison to their fast thermocouple sensor on a slower aircraft, the unheated Rosemount sensor underestimated the flux by about 21% in their measurements. The magnitude of the correction applied here is thus reasonably consistent with expectations from that study.

By obtaining a realistic measurement of the cospectrum at high frequency, it is possible to estimate how much of the otherwise unknown contribution above 1 Hz has been missed and therefore to judge if the frequency coverage is adequate. In this case, the exceedance curve is less than 2% at 10 Hz and falls rapidly above that frequency, even after correction, so it appears likely that additional contributions from higher frequencies can go unmeasured without introducing serious errors into the measurement of flux.

4.3 Evidence from Simulated Measurements

This section uses simulated measurements with the analysis methods described in the preceding section to demonstrate that those correction schemes can recover the assumed simulated conditions. The study uses generated time series representing isotropic wind measurements that have a specified relationship to the eddy dissipation rate and the expected $-5/3$ slope of spectral variance vs. frequency that is expected for an inertial sub-range. The procedure was to generate a Gaussian-noise spectrum, find the Fourier components, weight them to obtain a $-5/3$ slope, and then use an inverse Fourier transform to reconstruct the simulated measurement series. To provide a more realistic representation of the variance spectra often observed, the spectral variance is attenuated a low frequency to produce a peak variance at several-kilometer wavelength.

The variance spectrum expected for an inertial sub-range has the following form:

$$P(\nu) = C\left(\frac{2\pi}{V}\right)^{-2/3} \varepsilon^{2/3} \nu^{-5/3} \tag{17}$$

[8]The cumulative distribution termed "exceedance" here is sometimes called the ogive.

where $C = 0.5$ for the longitudinal component of the wind and 2/3 for a lateral component. An eddy dissipation rate of $10^{-3}\,\mathrm{m^2 s^{-3}}$ and a flight speed of $V = 200$ m/s were used with (17) to specify the desired variance spectrum.

Thirty-minute time series were generated for the three components of the wind, for an eddy dissipation rate of $10^{-3}\mathrm{m^2 s^{-3}}$, and then long-wavelength components with frequency below 0.05 Hz were attenuated by multiplying the Fourier components by $\exp(-5 * 0.05/|\nu|)$ where ν is the frequency. This not only produced a more realistic spectrum but also improved the accuracy of the high-frequency simulation, which otherwise exhibited some variability for different random sequences.

To generate sensible-heat flux a correlation was introduced between the simulated temperature and updraft, as follows:

1. In addition to the three-component time series for the wind, another independent time series with the same slope was generated for the *air temperature* T_a with fluctuations T_a' scaled smaller by a factor of $S = 1^\circ\mathrm{C}/(5\,\mathrm{m/s})$ in comparison to the magnitude of the wind fluctuations.

2. Correlation between the two time series was then introduced by defining a new temperature time series with the fluctuations $T_c' = (1-r)T' + rw'S$ where $r = 0.3$. The result will be $< w'T_c' >= r\sqrt{\sigma_w \sigma_{T_c}}$, which will lead to a flux of sensible heat specified as

$$F_s = \rho_a C_p r \sqrt{\sigma_w \sigma_{T_c}}$$

3. Finally, the measured recovery temperature was simulated by adding the dynamic-heating correction to the simulated air temperature and then filtering the result to represent how the sensor would respond.

In this simulation, the correlation is the same at all frequencies so the contribution to the measured flux also extends over all frequencies, with decreasing contributions as frequency increases. About 15% of the $< 2.5\,\mathrm{km}$ flux is contributed by frequencies above 1 Hz, where the sensor may respond incompletely to the fluctuations and underestimate the flux.

Figure 12 shows (as the green line) how the simulated cospectrum would be measured by a sensor with response parameters $\{a, \tau_1, \tau_2\}$ equal to $\{0.733, 0.0308, 0.447\}$, as is characteristic of a Rosemount 102E4AL sensor. The simulated measurement of air temperature was obtained by adding the dynamic-heating correction to the simulated air temperature and then applying the digital filter developed in Part 2 to estimate how the sensor would respond. Then the resulting value for measured recovery temperature was corrected for dynamic heating to obtain the value that would be measured for the air temperature, and that value was used with the simulated updraft to calculate the cospectrum. The resulting measured cospectrum is significantly smaller than the generated cospectrum for frequencies above about 1 Hz and is almost a factor of ten too low at 10 Hz. The measured exceedamce distribution (dashed brown line) emphasizes the extent of the missing flux at high frequency.

The cospectrum obtained using the correction procedure of Sect. 4.1 was consistent with the generated cospectrum, as illustrated by the corrected exceedance distribution in Fig. 12 (dashed

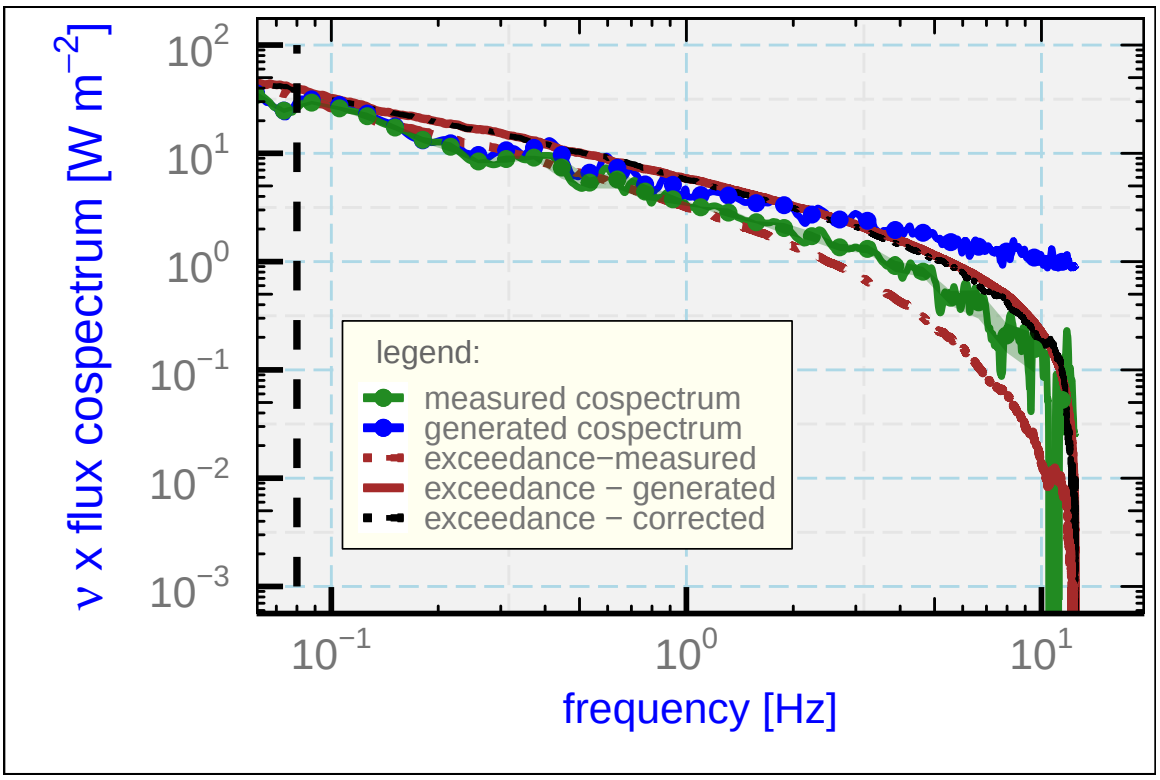

Figure 12: The cospectrum for the flux of sensible heat (blue line), weighted by frequency ν, for the simulated data generated as described in the text. Three 10-min segments of simulated 25 Hz data were averaged. The measured cospectrum was obtained by filtering the simulated recovery temperature and subtracting the correction for dynamic heating. For the generated and measured cospectrum, filled circles indicate the average values calculated in 50 logarithmically space intervals, and for the measured cospectrum shading indicates the standard deviation in those intervals. The exceedance lines show the contribution to flux from frequencies higher than the plotted frequency. The corrected cospectrum is not shown but is consistent with the generated cospectrum, as demonstrated by the agreement between the generated exceedance and the corrected exceedance. The units for the exceedance distributions are W m^{-2}, while the units for the weighted flux cospectra are W m^{-2} per unit logarithmic increment.

black line). For wavelengths smaller than 2.5 km, the generated flux of sensible heat was 39.5 $\mathrm{W\,m^{-2}}$, the measured values before and after correction were 33.2 and 38.5 $\mathrm{W\,m^{-2}}$. The correction thus reduces the 15% measurement error to about 2.5%. The representation of the high-frequency contribution is improved significantly by the correction procedure: For the contribution to the flux from frequencies above 3 Hz, the respective values for the generated, measured, and corrected exceedance distributions are 15.3, 10.8, and 15.1 $\mathrm{W\,m^{-2}}$, so about 30% of the contribution in this frequency range would be missed without correction.

This test only confirms consistency between the prediction of the transfer function and the correction procedure based on that function. The former, when deployed in a digital filter, is dependent on the assumptions and weaknesses in that filter, while the latter may be influenced by end effect and window effects from calculating the Fourier transforms. The agreement between the simulated and corrected flux therefore provides some support for the filter developed in Part 2 and for the correction procedure developed in this paper.

5 Summary and Conclusions

The key findings are these:

1. The differential equations (3) and (4), with appropriate parameters, provide an analytical representation of the transfer function for the recovery temperature measured by an unheated Rosemount 102E4AL sensor. That transfer function was shown to be consistent with measurements of the phase and amplitude ratio of the response to dynamic-heating fluctuations. This is good evidence that the equations provide a good representation of the time response for that sensor. The predictions of the equations are less satisfactory when applied to a heated HARCO sensor or a heated Rosemount sensor, possibly indicating that the heat transfer is not represented adequately by those equations.

2. For the Rosemount 102E4AL sensor, the three parameters in those equations (characterizing the two time constants and the fraction of heat transfer to the air vs. that to the structure supporting the sensing wire) can be determined with small uncertainty by fitting the transfer function to observations of dynamic heating. These parameters are thus constrained well and can be relied upon to make corrections to the measurements and otherwise to characterize the effects of time response of that sensor.

3. Once the transfer function for the unheated Rosemount sensor has been determined, it can be used to estimate the true recovery temperature, and then transfer functions for other sensors can be determined by comparison to that estimate of the measurand to which they are responding. This approach has been used here for the slower heated sensors and should provide a means of correcting other sensors slower than the unheated sensor. Appendix A uses these results with standard methods to correct the measurements from airborne temperature sensors for their time response.

4. Because temperature sensors often do not respond fast enough to measure high-frequency components of the dynamic-heating correction, erroneous corrections are introduced by conventional data processing. Instead, the corrections should be filtered to match the response of the temperature sensor to avoid introduction of these errors. A digital filter is proposed that can be used to correct standard processing schemes to eliminate the errors arising from the dynamic-heating term. The errors discussed here are prevalent in almost all existing data from research aircraft, so application of this proposed correction method will lead to significant improvement in those measurements.

5. A correction procedure was proposed that consists of using the transfer function to calculate the sensible-heat flux. Three cases are presented, all with significant correlation between temperature and updraft at a range of frequencies including those above 1 Hz. The measured values of sensible-heat flux would be underestimated significantly (by about 40%, 30%, and 44% in the three cases) without correction.

6. The cospectrum with correction appears to be represented reasonably at frequencies up to about 10 Hz, so the rapidly decreasing concentration to the cospectrum from these frequencies suggests that it is not necessary to measure contributions from frequencies

above this limit. This conclusion is tentative and needs reconsideration when applied to new cases.

7. Results of a simulation support the consistency between the response as represented by the digital filter and the application of the transfer function to correct the measurement of the flux of sensible heat.

A Correcting the Temperature

The true recovery temperature T_r can be retrieved from the measured temperature T_m in two ways, either from the differential equations or by Fourier transformation. These methods are illustrated here.

The differential equations (3) and (4) provide a basis for correcting the measured temperature to account for the time response of the sensor. They should be applied to the recovery temperature $T_r(t)$, which is the measurand. The actual measurement is $T_m(t)$ and the temperature of the support is $T_s(t)$, so those equations, rearranged, are:

$$\frac{dT_s(t)}{dt} = \frac{T_r(t) - T_s(t)}{\tau_2} \tag{18}$$

$$T_r(t) = \frac{1}{a}\left\{\tau_1 \frac{dT_m(t)}{dt} + T_m(T) - (1-a)T_s(t)\right\} \tag{19}$$

There are two unknowns ($T_r(t)$, the actual recovery temperature, and $T_s(t)$). Those unknowns are specified by the two preceding equations because all other terms are known, including dT_m/dt which can be represented using the numerical derivative of the measurements $T_m(t)$. The second equation can be used to eliminate T_r from the first:

$$\frac{dT_s(t)}{dt} = \frac{\frac{1}{a}\left\{\tau_1 \frac{dT_m(t)}{dt} + T_m(T) - (1-a)T_s(t)\right\} - T_s(t)}{\tau_2} \tag{20}$$

From an initial value $T_s(0)$, assumed to be $T_m(0)$, this equation can be integrated to find the temperature of the support, $T_s(t)$. Once that is known, (19) specifies the estimate of the true recovery temperature $T_r(t)$ without further integration. The only choices needed are the numerical method used to find the derivative dT_m/dt (e.g., here centered fourth-order) and the integration method applied to (20), here fourth-order Runge-Kutta integration with Cash-Karp (Cash and Karp [1990]) adjustment of the step size. If a centered second-order finite-difference expression is used for $dT_m(t)/dt$ and an Euler integration is used to integrate (20), this correction can be shown to be equivalent to that developed by Inverarity [2000]; cf. his Eqn. (12). However, the correction should be applied to the recovery temperature, not the air temperature. The sensor responds to the recovery temperature, which includes the increase caused by dynamic heating. Applying the correction to the recovery temperature properly corrects the response to dynamic heating also, so the dynamic-heating correction can then be subtracted from the corrected recovery temperature to obtain an estimate of the air temperature.

An alternate approach is to use Fourier transforms:

1. Calculate the Fourier transform of the measured time series: $\hat{T}_m(\omega) = \mathscr{F}\left(T_m(t)\right)$ where ω is angular frequency and $\mathscr{F}$ denotes the Fourier transform.
2. Divide the result by the complex representation of the transfer function: $\hat{T}_r(\omega) = \hat{T}_m(\omega)/H(\omega)$.
3. Use the inverse Fourier transform to find a retrieved estimate of the true recovery temperature: $T_r(t) = \mathrm{Re}\left(\mathscr{F}^{-1}\left(\hat{T}_r(\omega)\right)\right)$ where Re denotes the real part of the complex result.

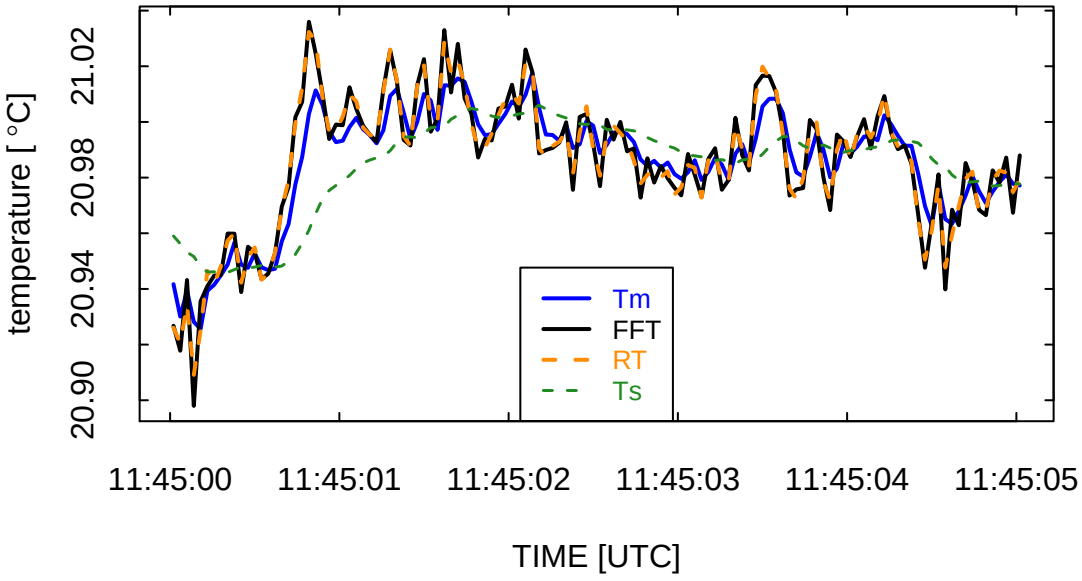

Figure 13: Example of the changes produced by the correction procedures. The original measurement of recovery temperature is Tm, produced by an unheated Rosemount sensor, and the revised values are RT (from integration) and FFT (from Fourier transforms). The dashed green line labeled "Ts" is the temperature of the support as calculated using (17). Measurements from VOCALS flight 3.

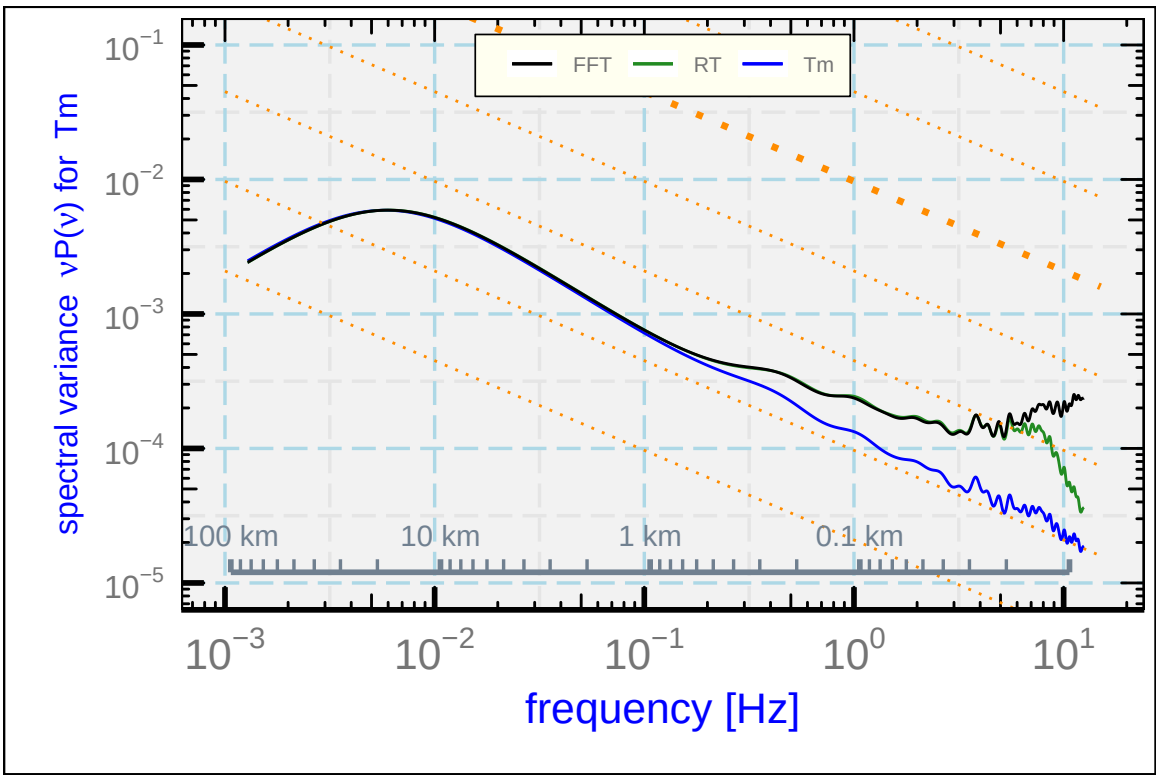

Figure 14: Variance spectra for the original measurement of recovery temperature (Tm) produced by an unheated Rosemount sensor and for the corrected values (RT and FFT) produced respectively by (16) and the Fourier-transform algorithm.

Sample results of these correction procedures are shown in Fig. 13. The agreement between the two correction methods is very good, and both show evidence of faster and higher-amplitude response to fluctuations. The resulting variance spectrum for the Fourier-transform method (Fig. 14) has high variance above about 5 Hz that is above the variance for the corrected variable obtained from (19). The increasing variance for the Fourier-transform method is is likely the fault of the measurement itself: The spectral variance for the original measurement (Tm) does not decrease at high frequency as expected from the transfer function, and the correction procedure amplifies this excess noise. The lower variance for the variable obtained from (19) at high frequency arises from the finite-difference representation of the term $dT_m(t)/dt$, which results in some smoothing.

Because the heated HARCO sensor is much slower than the unheated Rosemount 102E4AL sensor, the measurements from that slower sensor can't be corrected to the extent possible for the unheated sensor, but it is still useful to evaluate to what extent the measurements can be improved. The HARCO presents a special case because the best-fit value is $a = 0$ so (19) can't be used. However, in this case the differential equations can still be combined to give

$$T_r(t) = (\tau_1 + \tau_2)\frac{dT_m(t)}{dt} + T_m(t) + \tau_2\tau_1\frac{d^2T_m(t)}{dt^2} \tag{21}$$

a form that can be used directly without integration because finite-difference expressions can be used for the derivatives of the measured $T_m(t)$. The solution from (21) is very noisy if finite-difference estimates of the derivatives are used, so smoothing of the result was applied. Figure 15 shows the result (as "RTH") after a Butterworth low-pass filter with cutoff frequency of 2 Hz smoothed the corrected measurements. This filtering is reasonable because the variance spectrum for this sensor shows very little real signal at frequencies above 2 Hz. In comparison to the original measurement (labeled "Tm"), the response of the sensor is greatly improved by this correction procedure. It even provides a reasonable representation of the corrected unheated Rosemount measurement (labeled "RT") for the same period.

This is not as good a representation of the transfer function as is possible with the fitted representation shown in Fig. 4 and given by (12). That fit can be used with the Fourier-transform approach to correction. The result is shown in Fig. 15 as the black line labeled "FFT". This is also a significant improvement over the original and reproduces many of the features of the best measurement ("RT"). To obtain this result, it was necessary to attenuate frequencies above 1.8 Hz in the Fourier transform solution because there is a zero in the transfer function as represented by (12) that otherwise invalidates the inversion. This attenuation was accomplished by multiplying the transfer function by $e^{5\nu}$above 1.8 Hz. This arbitrarily chosen attenuation gave reasonable results, although it is likely that better choices could be made with further exploration. One more general measure of the improvement, beyond the anecdotal evidence in the preceding figures, is that either correction procedure reduced the standard deviation of the difference between the measured value (Tm) and the estimated best value (RT) from 0.06°C before correction to 0.03°C after correction.

The plot of variance spectra (Fig. 16) shows that the original spectrum (blue line labeled "Tm") is seriously attenuated at high frequencies relative to the reference measurement ("RT") and that both correction procedures restore significant parts of the missing spectral variance. Despite its inferior representation of the transfer function, it appears that application of 21 provides a

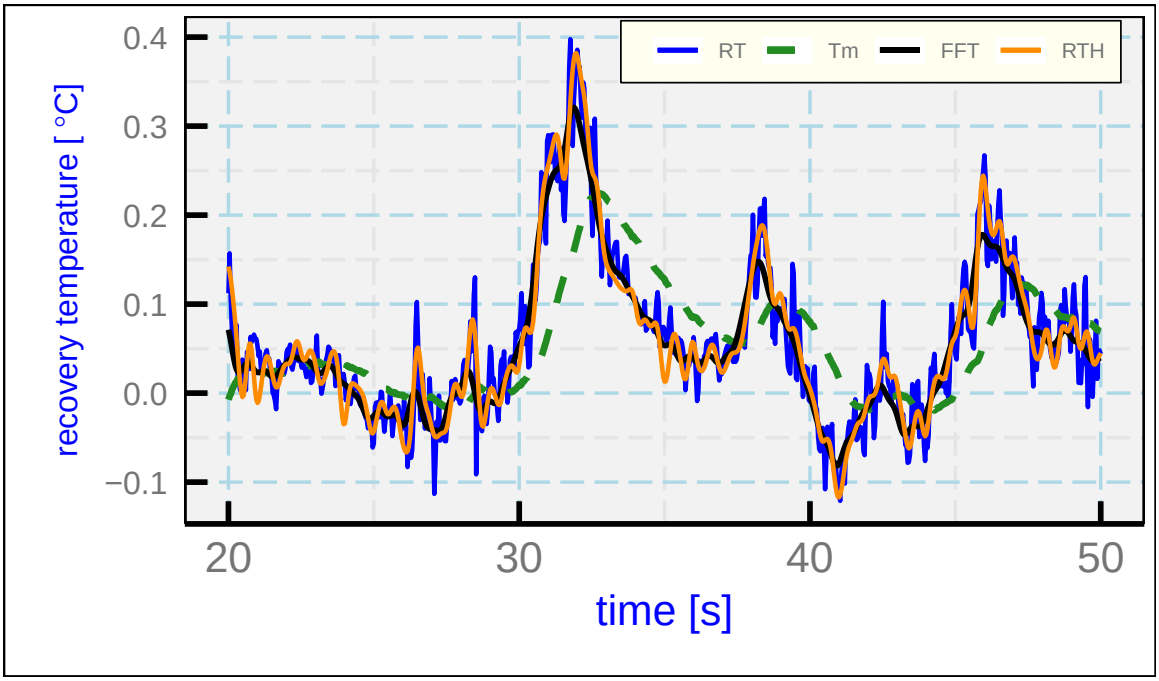

Figure 15: Corrected recovery temperature as measured by a heated HARCO sensor ("RTH" and "FFT"), the uncorrected measurement ("Tm"), and the best estimate of the true recovery temperature ("RT") based on an unheated Rosemount sensor after correction. The time is seconds after 2018-02-24 5:59:00 UTC, SOCRATES flight 15. "RTH" is based on the approximate formula (20), while "FFT" results from Fourier transformation after correction using the transfer function determined from (13). Mean values have been subtracted from all to facilitate comparisons.

better match to the reference measurements. It does not appear possible to restore the missing high-frequency fluctuations (above about 1 or 2 Hz) because the original measurement is so severely attenuated at these frequencies. This sensor and the similar heated Rosemount sensor are therefore unable to detect contributions to sensible-heat flux from this frequency range, even after corrections. It nevertheless appears useful to apply one of these correction approaches routinely to improve the quality of this measurement.

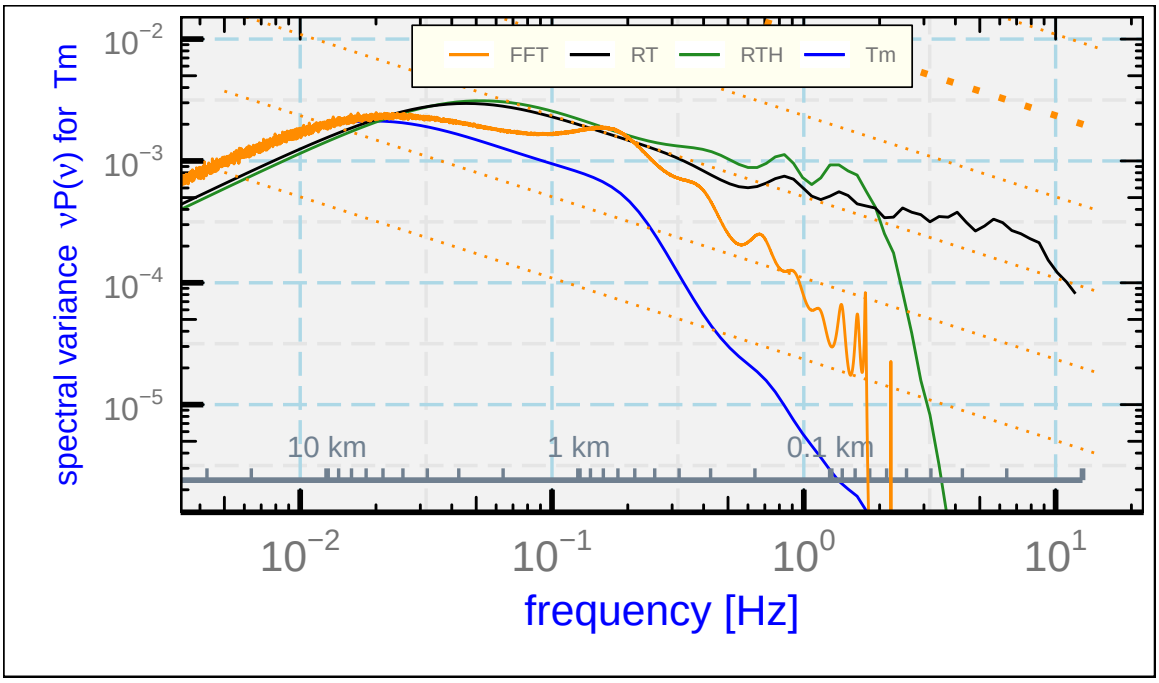

Figure 16: Variance spectra for some measurements of recovery temperature: "RT" (the best estimate resulting from correction of the measurements from the unheated Rosemount 102E4AL); "Tm" (the uncorrected measurement from the heated HARCO); "FFT" (the corrected HARCO measurement based on Fourier transforms); and "RTH" (the corrected HARCO measurement based on the correction formula (17)).

B The Digital Filter for Dynamic Heating

As described in Sect (3.1), digital filters for dynamic heating were developed from the transfer functions for the probes studied in Part 1. The procedure was to use the inverse Fourier transforms of those transfer functions, which give the impulse response functions, and then design filters using coefficients determined from those impulse functions. This appendix describes in more detail how this was done and includes references to the coefficients that might be used by others. The filters so obtained appear to function as desired, although this is an area where further work will be warranted.

The procedures was as follows:

1. Specify the transfer function for the sensor (e.g., for the unheated Rosemount 102E4AL sensor or the heated HARCO sensor) as determined in Part 1.

2. For a large set of frequencies spanning the interval from -12.5 to 12.5 Hz, e.g., with resolution between assumed frequencies of (1/600) Hz, evaluate the frequency-dependent transfer function. This solution is stored in a vector with frequencies in the order (0 to 12.5 Hz, then $(-12.5+1/600)$ to $-(1/600)$ Hz, as is conventional for representations of the Fourier transform in R and also many other languages. It was necessary to calculate the negative-frequency components and, to obtain real-number results, to store them so that the values representing negative frequencies are complex conjugates of those for the corresponding positive frequencies.

3. The inverse Fourier transform then gave the impulse function at 15,000 delays, many of them representing negative delays. The values in the central part of this array were mostly very small.

4. To obtain a manageable number of moving-average coefficients, all values in the array representing the impulse function were set to zero for indices k with values $M+2 \leq k \leq N-M$ where N is the length of the calculated impulse function and $M = 100$, which left 201 non-zero coefficients. These coefficients then spanned 8 s at 25 Hz, a time long compared to the expected impulse response of the sensor.

5. The upper-100 coefficients represent negative delays in the impulse response because of the cyclic nature of the Fourier transform, so the coefficients were re-arranged into a sequence with the last-100 coefficients first and the initial-101 coefficients moved to the end of the array. These coefficients were then moving-average coefficients that implement a filter matching the transfer function, except for the omitted terms outside the 200-coefficient range that are assumed negligible.

6. The resulting set of moving-average coefficients can then be applied to the measured dynamic-heating term Q to produce a filtered version.

7. The filtered result then needs to be shifted in time by 4 s to correct for the offset in the filter.

Additional details, references to filter coefficients, and relevant R code are included in the "Workflow" document.

C Pressure-Line Resonance

Cooper et al. [2016] showed evidence that the variance spectrum of the longitudinal component of the wind measured by the NSF/NCAR GV appears to have excess variance at frequencies above about 2 Hz. Figure 17 shows the problem: Both the airspeed and the dynamic heating calculated from it have excess variance above the expected distribution for frequencies above about 2 Hz, although this is a turbulent region with characteristics otherwise consistent with an inertial subrange. The lateral components of the wind do not show this excess variance; it only appears in the longitudinal component. It is far above the noise expected from the precision of the sensor used to measure the dynamic pressure (estimated at about 0.1 hPa), so there must be another source of this contamination of the signal. A similar but less pronounced effect on a different aircraft was shown by Nicholls [1978] (in his Fig. 2) and was also discussed by Inverarity [2000]. Both references used filtering of the final temperature measurement to give a reasonable variance spectrum, but it will be argued here that the effect should be removed from the dynamic-heating correction instead.

The suggested explanation (by D. Lenschow, included in Cooper et al. [2016], p. 140) is that there is resonance in the lines connecting the pressure ports to the pressure transducers and effects in those lines cause either amplification or attenuation of the pressure signals, along with phase shifts, at various frequencies. On the NSF/NCAR GV dynamic pressure is measured by a differential pressure transducer that connects to a pitot-tube and, on the reference side, to the static-pressure ports. The connecting lines are about 8-m long to the static-pressure sources and a few meters long to the pitot tube. The extraneous variance in the pressure lines does not influence the temperature sensor. Therefore, subtraction of the measured dynamic-heating term from the recovery temperature to obtain the ambient temperature introduces still more high-frequency noise into the measurement of air temperature if the estimate of dynamic heating is contaminated by these line effects. When correcting for temperature-sensor time response, this additional source of false variation in the dynamic-heating term should be removed where possible. This appendix discusses a possible approach to that removal.

The argument presented in Cooper et al. [2016] was that line resonance in the static pressure line used as a lower-pressure reference for the dynamic-pressure measurement was responsible. It appears now that this was not the correct explanation. The reason is that fluctuations in static pressure normally make a negligible contribution to the measured fluctuations in dynamic pressure; instead, fluctuations in dynamic pressure are dominated by fluctuations in the total pressure delivered by the pitot tube to the differential sensor. Figure 18 shows that the dominant contributions to variance in dynamic pressure, measured as the difference between the total and static pressure, comes from the variance in the total pressure present in the shorter inlet line. Resonances in both lines need to be evaluated, but the following analysis indicates that the fluctuations in the static-pressure line do not make any significant contribution to fluctuations in measured dynamic pressure.

Lenschow's analysis (based on theoretical predictions of Iberall [1950]) leads to a transfer function representing the effect of the line resonance on the measurement. This transfer function was plotted in Fig. 52 of Cooper et al. [2016] and has been recalculated from the equations in Iberall [1950], specifically Eqs. (105) and (106) with (99) and (95) from that reference and with the

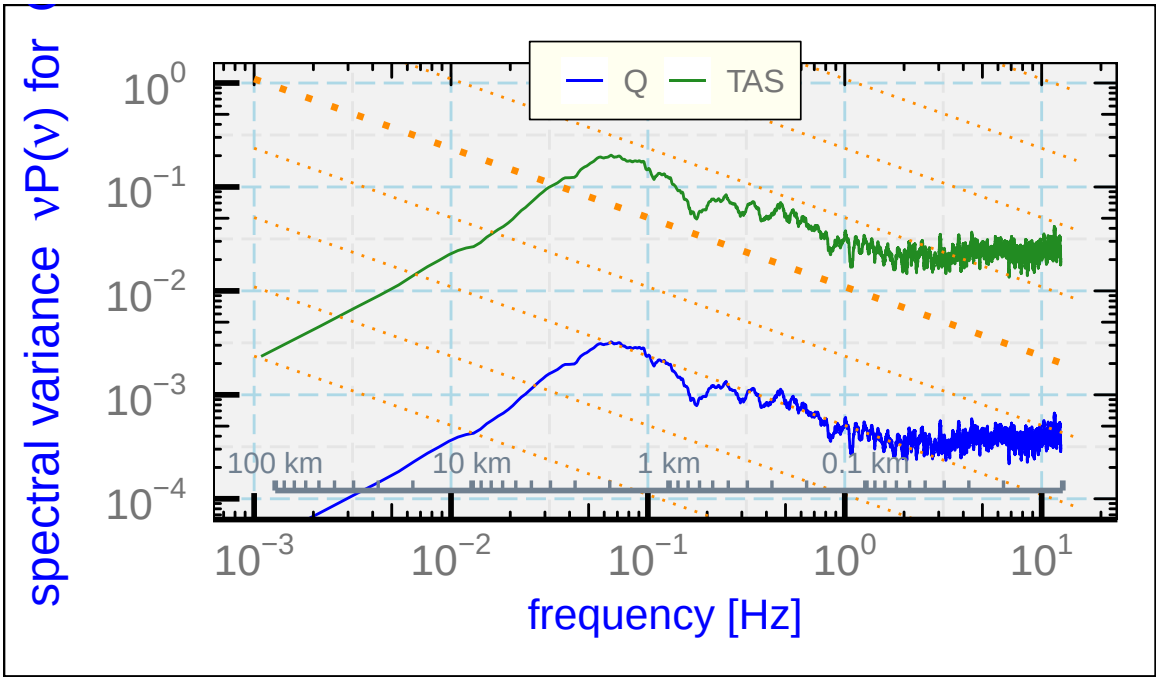

Figure 17: The variance spectrum for the dynamic-heating correction Q, from SOCRATES flight 15, 6:00:00 to 6:15:00 UTC, in a region thought to have characteristics of an inertial subrange. The variance spectrum for the airspeed measurement (TASX) is also shown.

volume within the pressure sensor at the end of the line assumed to be 300 mm^3 as used by D. Lenschow, for use in the present work. That transfer function then can be used in the same way as the time-response transfer function to correct the measured dynamic-heating term by applying the correction to both lines connected to the dynamic-pressure sensor. The result should be a better estimate of the dynamic heating at the temperature sensor because the fluctuations occurring only in the lines and not affecting the temperature sensor will be removed.

Consider first the effect on static pressure. The predicted transfer function is based on a theoretical analysis, so it is useful to determine from observations if the correction based on that transfer function is reasonable. In a region thought to represent an inertial subrange, the slope of the variance spectrum of the longitudinal wind (and therefore of airspeed fluctuations and also the dynamic-heating term) is expected to exhibit a $-5/3$ slope with frequency or a $-2/3$ slope in the frequency-weighted spectral-variance plots used here. Measurements of static pressure from the same region shown in Figs. 17 and 18 were processed by calculating the Fourier transform of the pressure, dividing by the transfer function, and using an inverse Fourier transform to recover the corrected pressure. The result is shown as "PSC" in Fig. 19, as the green line (mostly overlapped at low frequency by the black line). The result seems reasonable for frequencies below about 8 Hz, but there is a sharp increase above that point. Two possible causes are: (i) The sensor resolution, thought to be 0.1 hPa from the manufacturer's specified uncertainty limit, would cause a noise spectrum of about this magnitude, although with a smaller slope; and (ii) aliasing of higher-frequency fluctuations may contribute. The digital filters applied to the measurements don't remove this aliasing because the fluctuations are real fluctuations in pressure in the pressure lines and so will still be sampled as aliased. For these reasons, addi-

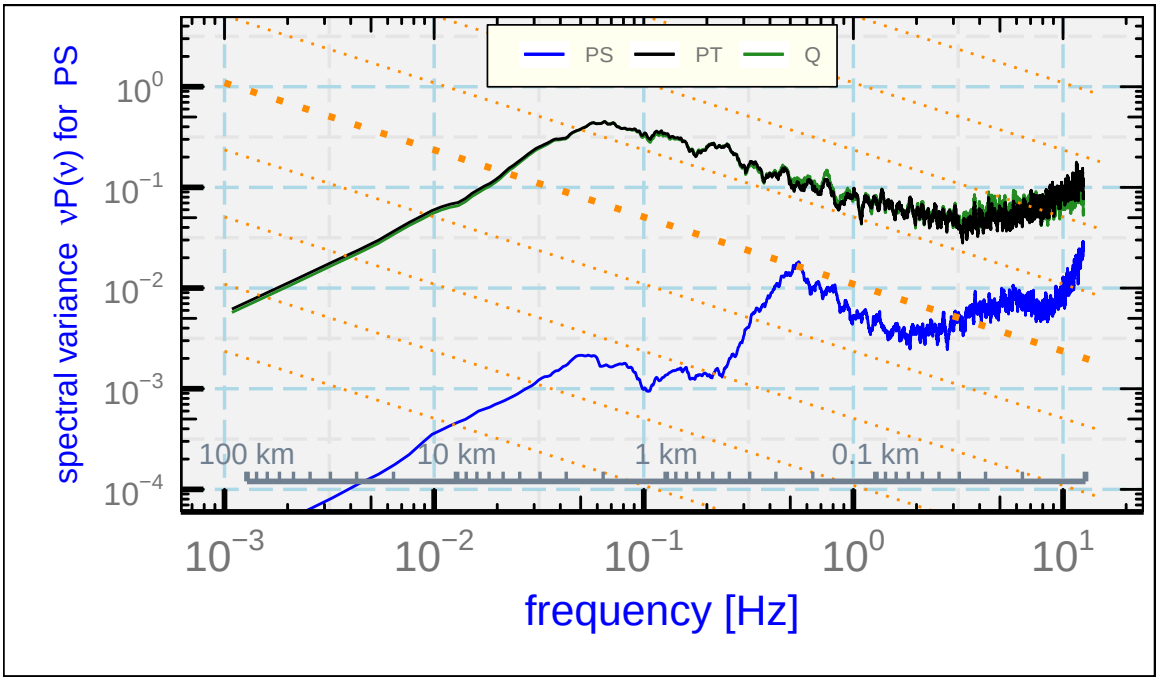

Figure 18: Variance spectra for three pressure measurements: the ambient or static pressure ("PS"), the dynamic pressure ("Q"), and their sum ("PT"), the total pressure. The plots for dynamic and total pressure mostly overlap and are indistiguishable in this plot.

tional filtering was applied to the Fourier components before inverse transformation to reduce frequencies above 8 Hz. The result, shown as "PSFR" in the figure, is a reasonable adjustment to the original variance spectrum to account for line resonance for frequencies below 8 Hz, and evidently excess variance at higher frequency has been removed

This approximate agreement between predictions for the measured static pressure and the expected shape of the variance spectrum after correction, for frequency below 8 Hz, provides some support for the theoretical analysis by greatly improving the appearance of the variance spectrum for pressure, although the shape is still not ideal. The spectrum would appear better if the gain of the transfer function around 4 Hz were approximately 40% larger so that the variance there would be reduced by about a factor of 2. Although the distance from the static source to the pressure transducer is only about 3 m, it appears that resonance in the branch of this line that continues forward to the differential transducer affects the signal also at this location.

Analysis of the effect of line resonance on the measurement of dynamic pressure is more complicated because resonance can occur in both lines, the line delivering total pressure from the pitot tube and the line delivering static pressure from the static sources. The measured quantity at the differential pressure transducer is the difference between the total-pressure-line resonating pressure and the ambient-pressure-line resonating pressure, so (using primes to denote quantities in the resonating lines) $p'_t = q' + p'_s$ is the true total pressure in the line from the pitot tube. This can be corrected using the theoretical transfer function for that line[9] to obtain the true total

[9] Assumed parameters are length 4 m, diameter 3.1 mm, sensor volume $10^4\,\mathrm{mm}^3$. These need confirmation and possible adjustment. They were selected primarily to produce the appropriately corrected variance spectrum for

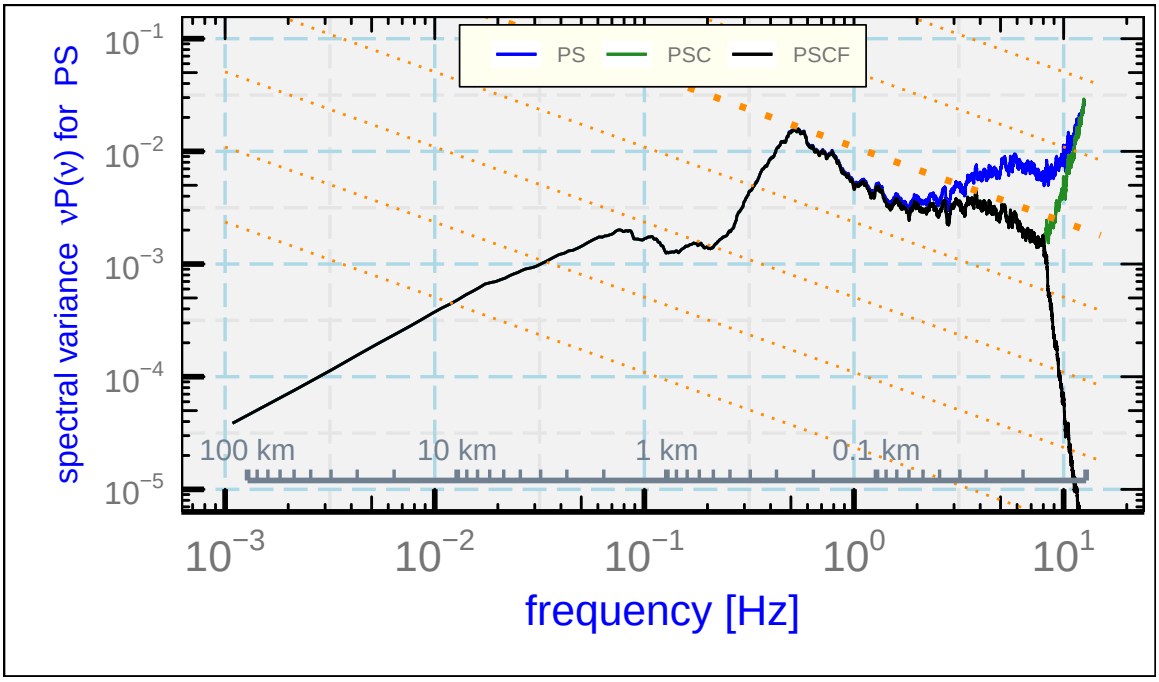

Figure 19: The variance spectrum that results from correcting the measured static pressure ("PS") for the theoretical effect of line resonance. The corrected pressure is represented here as "PSC". To reduce suspected noise, additional attenuation is applied above 8 Hz to obtain "PSCF".

pressure at the inlet to the pitot tube, p_t. Then the best estimate of the true dynamic pressure q is $q = p_t - p_s$ where corrected quantities are used for both p_t and p_s, the latter as estimated from "PSCF" in Fig. 19. The corrected measurement of dynamic pressure, shown as "QC" in Fig. 20, now exhibits a variance spectrum with the expected high-frequency slope.

This correction greatly improves the variance spectrum for dynamic pressure by giving a slope consistent with expectations for an inertial subrange. During this flight segment, other measurements (notably the vertical wind) indicate $-5/3$ slope, while the uncorrected measurement departs from that slope significantly for frequencies above about 4 Hz. Using this corrected dynamic pressure produces a longitudinal component of the wind having a spectrum consistent with the lateral components. The excess variance present at these frequencies therefore should also be removed from estimates of dynamic heating based on dynamic pressure, before the filtering to account for temperature-sensor response (Sect. (3.1)) is applied, because the temperature sensor in a separate housing is not affected by the fluctuations that are removed.

dynamic heating. The sensor volume in particular is probably too high.

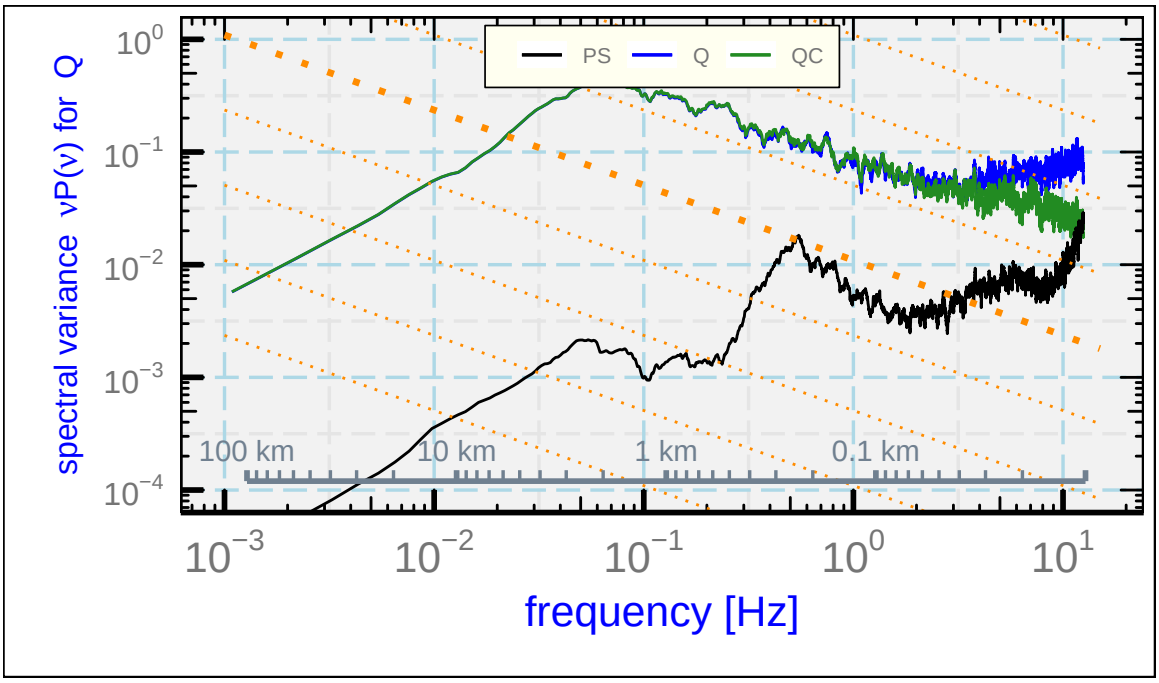

Figure 20: Variance spectra for the best estimate for dynamic heating, "QC", after correction for resonance in both lines connected to the differential pressure sensor that produces the original measurement "Q". The corresponding spectrum for the measured pressure in the line connected to the static sources ("PS") is also shown.

D Reproducibility

This document is constructed in ways that support duplication of the study. The code that generates the plots and implements the correction procedure is incorporated into the same file that generated this document via LaTeX, using principles and techniques described by Xie [2013] as implemented in the R package 'knitr' (Xie [2014]). The program, 'Paper1.Rnw', is archived on 'GitHub' in the directory at this URL. There is some supplemental material in that directory, including a workflow document for all the papers, the bibliography and some code segments saved in the "chunks" subdirectory, so the full directory should be downloaded in order to run the program. The calculations use the programming language R (R Core Team [2019]) and were run within RStudio (RStudio [2009]), so this is the most straightforward way to replicate the calculations and the generation of this document.

A package named Ranadu, containing auxillary functions, is used extensively in the R code. It is available on GitHub as https://github.com/WilliamCooper/Ranadu.git. The version used for calculations in this technical note is included in the 'zip' archive listed below.

The data files used are also preserved in the NCAR/EOL Data Archives and can be obtained via a request to `mailto:raf-dm@eol.ucar.edu` or via the "Data Access" links at this web site. The original files containing the data as produced by the NCAR Earth Observing Laboratory, Research Aviation Facility, were in netCDF format (cf. this URL), but in many cases data archives were reprocessed and the files may change after reprocessing so a separate archive is maintained for this document. The data files in this archive contain R data.frames and are preserved as binary-format 'Rdata' files via R 'save' commands. The code in the GitHub archive has appropriate 'load' commands to read these data files from a subdirectory named 'Data' (/Data or ~/Data or /home/Data) but this is not part of the GitHub repository because it is too large to be appropriate there. To reproduce this research, those data files have to be transferred separately from {??where??}

Extensive use has been made of attributes assigned to the data.frames and the variables in those data.frames. All the attributes from the original netCDF files have been transferred to the data.frames, so there is a record of how the original data were processed, for example with calibration coefficients and processing dependence for the variables. Key information like the processing date, the program version that produced the archive, and the selection of primary variables for various measurements thus is preserved.

(See the related list of project components on the next page that are preserved to enhance reproducibility.)

PROJECT:	SensibleHeatFlux
ARCHIVE PACKAGE:	SensibleHeatFluxPaper1.zip
CONTAINS:	attachment list below
PROGRAM:	Paper1.Rnw
ORIGINAL DATA:	UCAR/NCAR - Earth Observing Laboratory [2011], UCAR/NCAR - Earth Observing Laboratory [2017], ,UCAR/NCAR - Earth Observing Laboratory [2019]
SPECIAL DATA FILES:	SensibleHeatFluxTechNote.Rdata, SensibleHeatFluxTechNote2.Rdata
WORKFLOW DOCUMENT:	WorkflowSensibleHeatFlux.pdf
GIT:	https://github.com/WilliamCooper/SensibleHeatFlux.git

Attachments:
Paper1.Rnw
Paper1.pdf
WorkflowSensibleHeatFlux.pdf
WAC.bib
chunks/*
SessionInfo

References

Bruce Albrecht, Virendra Ghate, Johannes Mohrmann, Robert Wood, Paquita Zuidema, Christopher Bretherton, Christian Schwartz, Edwin Eloranta, Susanne Glienke, Shaunna Donaher, et al. Cloud system evolution in the trades (cset): Following the evolution of boundary layer cloud systems with the nsf–ncar gv. *Bulletin of the American Meteorological Society*, 100(1):93–121, 2019. (document), 2.3, 2.4.1

Jens Bange, Marco Esposito, Donald H. Lenschow, Philip R. A. Brown, Volker Dreiling, Andreas Giez, Larry Mahrt, Szymon P. Malinowski, Alfred R. Rodi, Raymond A. Shaw, Holger Siebert, Herman Smit, and Martin Zöger. *Measurement of Aircraft State and Thermodynamic and Dynamic Variables*, chapter 2, pages 7–75. John Wiley & Sons, Ltd, 2013. ISBN 9783527653218. doi: 10.1002/9783527653218.ch2. URL https://onlinelibrary.wiley.com/doi/abs/10.1002/9783527653218.ch2. 2.2

Jeff R Cash and Alan H Karp. A variable order runge-kutta method for initial value problems with rapidly varying right-hand sides. *ACM Transactions on Mathematical Software (TOMS)*, 16(3):201–222, 1990. 5, A

W. A. Cooper, S. M. Spuler, M. Spowart, D. H. Lenschow, and R. B. Friesen. Calibrating airborne measurements of airspeed, pressure and temperature using a doppler laser air-motion sensor. *Atmospheric Measurement Techniques*, 7(9):3215–3231, 2014. doi: 10.5194/amt-7-3215-2014. URL http://www.atmos-meas-tech.net/7/3215/2014/. 2.3

W. A. Cooper, R. B. Friesen, M. Hayman, J. B. Jensen, D. H. Lenschow, P. A. Romashkin, A. J. Schanot, S. M. Spuler, J. L. Stith, and C. Wolff. Characterization of uncertainty in measurements of wind from the NSF/NCAR Gulfstream V research aircraft. NCAR technical note NCAR/TN-528+STR, Earth Observing Laboratory, NCAR, Boulder, CO, USA, jul 2016. URL http://n2t.net/ark:/85065/d7qr4zqr. 2.3, C, C, C

C. A. Friehe and D. Khelif. Fast-response aircraft temperature sensors. *J. Atmos. Ocean. Technol.*, 9(6):784–795, DEC 1992. ISSN 0739-0572. doi: 10.1175/1520-0426(1992)009<0784:FRATS>2.0.CO;2. 1, 2.1, 2.1, 2.3

A. S. Iberall. *J. Res. Natn. Bur. Stand.*, (45):85–108, 1950. doi: 10.6028/jres.045.008. URL http://nvlpubs.nist.gov/nistpubs/jres/045/jresv45n1p85_A1b.pdf. C

G. W. Inverarity. Correcting airborne temperature data for lags introduced by instruments with two-time-constant responses. *Journal of Atmospheric and Oceanic Technology*, 17(2):176–184, 2000. doi: 10.1175/1520-0426(2000)017<0176:CATDFL>2.0.CO;2. URL https://doi.org/10.1175/1520-0426(2000)017<0176:CATDFL>2.0.CO;2. 2.1, 2.6, 4.1, A, C

R. Paul Lawson and Alfred R. Rodi. A new airborne thermometer for atmospheric and cloud physics research. part i: Design and preliminary flight tests. *Journal of Atmospheric and Oceanic Technology*, 9(5):556–574, 1992. doi: 10.1175/1520-0426(1992)009<0556:

ANATFA>2.0.CO;2. URL https://doi.org/10.1175/1520-0426(1992)009<0556:ANATFA>2.0.CO;2. 1, 2.3, 4.2

D. H. Lenschow. The measurement of air velocity and temperature using the NCAR Buffalo Aircraft Measuring System. Technical report, 1972. URL http://nldr.library.ucar.edu/repository/collections/TECH-NOTE-000-000-000-064. 2.1

John McCarthy. A method for correcting airborne temperature data for sensor response time. *Journal of Applied Meteorology*, 12(1):211–214, 1973. 2.1, 2.1, 2.6, 4.1

GM McFarquhar, R Wood, CS Bretherton, S Alexander, C Jakob, R Marchand, A Protat, P Quinn, ST Siems, and RA Weller. The southern ocean clouds, radiation, aerosol transport experimental study (socrates): An observational campaign for determining role of clouds, aerosols and radiation in climate system. In *AGU Fall Meeting Abstracts*, 2014. (document), 2.3, 2.4.1

National Research Council. *The Atmospheric Sciences: Entering the Twenty-First Century*. The National Academies Press, Washington, DC, 1998. ISBN 978-0-309-06415-6. doi: 10.17226/6021. URL https://www.nap.edu/catalog/6021/the-atmospheric-sciences-entering-the-twenty-first-century. 1

S Nicholls. Measurements of turbulence by an instrumented aircraft in a convective atmospheric boundary layer over the sea. *Quarterly Journal of the Royal Meteorological Society*, 104 (441):653–676, 1978. 2.1, 2.6, 4.1, C

G. A. Payne, C. A. Friehe, and D. K. Edwards. Time and frequency response of a resistance-wire aircraft atmospheric temperature sensor. *Journal of Atmospheric and Oceanic Technology*, 11(2):463–475, 1994. doi: 10.1175/1520-0426(1994)011<0463:TAFROA>2.0.CO;2. URL https://doi.org/10.1175/1520-0426(1994)011<0463:TAFROA>2.0.CO;2. 2.1, 2.1

David Pierce. *ncdf4: Interface to Unidata netCDF (Version 4 or Earlier) Format Data Files*, 2015. URL https://CRAN.R-project.org/package=ncdf4. R package version 1.15. (document)

R Core Team. *R: A language and environment for statistical computing*. R Foundation for Statistical Computing, Vienna, Austria, 2019. URL http://www.R-project.org. (document), 4, D

AR Rodi and PA Spyers-Duran. Analysis of time response of airborne temperature sensors. *Journal of Applied Meteorology*, 11(3):554–556, 1972. 2.1

RStudio. *RStudio: Integrated development environment for R (Version 0.98.879)*, 2009. URL http://www.rstudio.org. (document), D

T. M. Stickney, M. W. Shedlov, and D. I. Thompson. Goodrich total temperature sensors. Goodrich Technical Report 5755 Revision C, Rosemount Aerospace Inc., 1994. URL http://www.faam.ac.uk/index.php/component/docman/doc_download/47-rosemount-report-5755(lastaccess:8Aug2014). 2.4.3

Bruce Swihart and Jim Lindsey. *rmutil: Utilities for Nonlinear Regression and Repeated Measurements Models*, 2019. URL https://CRAN.R-project.org/package=rmutil. R package version 1.1.3. (document), 5

UCAR/NCAR - Earth Observing Laboratory. NCAR/NSF C-130 navigation, state parameter, and microphysics HRT (25 sps) data. version 1.0 [data set, VOCALS], 2011. URL https://doi.org/10.5065/d69k48jk,Accessed09Jan2020. (document), D

UCAR/NCAR - Earth Observing Laboratory. High rate (hrt - 25 sps) navigation, state parameter, and microphysics flight-level data. version 2.0. [data set, CSET], 2017. URL https://doi.org/10.5065/D63R0R3W,Accessed12Mar2020. D

UCAR/NCAR - Earth Observing Laboratory. High rate (HRT - 25 sps) navigation, state parameter, and microphysics flight-level data. version 0.1 [preliminary] [data set, WE-CAN], 2018. URL https://data.eol.ucar.edu/dataset/548.004.Accessed09Jan2020. (document)

UCAR/NCAR - Earth Observing Laboratory. High rate (HRT) navigation, state parameter, and microphysics flight level data. version 1.0 [data set, SOCRATES], 2019. URL https://doi.org/10.26023/K5VQ-K6KY-W610,Accessed09Jan2020. (document), D

H. Wickham. *ggplot2: elegant graphics for data analysis*. Springer New York, 2009. ISBN 978-0-387-98140-6. URL http://had.co.nz/ggplot2/book. (document)

R Wood, CR Mechoso, CS Bretherton, RA Weller, BJ Huebert, F Straneo, Bruce A Albrecht, H Coe, G Allen, G Vaughan, et al. The vamos ocean-cloud-atmosphere-land study regional experiment (vocals-rex): goals, platforms, and field operations. 2011. (document), 2.3, 2.4.1

Y. Xie. *Dynamic Documents with R and knitr*. Chapman and Hall/CRC, Boca Raton, Florida, 2013. URL http://yihui.name/knitr/. ISBN 978-1482203530. (document), D

Y. Xie. *knitr: A general-purpose package for dynamic report generation in R*, 2014. URL http://yihui.name/knitr/. R package version 1.6. (document), D